haematologica
Journal of the Ferrata Storti Foundation

Immunomodulatory role of megakaryocytes in the hematopoietic niche of myeloproliferative neoplasms

by Xiaoxi Yang, Sandy Lee, Kyla Masarik, Tahmeena Ahmed, Lei Zheng and Huichun Zhan

Received: August 13, 2025.
Accepted: January 12, 2026.

Citation: Xiaoxi Yang, Sandy Lee, Kyla Masarik, Tahmeena Ahmed, Lei Zheng and Huichun Zhan. Immunomodulatory role of megakaryocytes in the hematopoietic niche of myeloproliferative neoplasms. Haematologica. 2026 Jan 22. doi: 10.3324/haematol.2025.288948 [Epub ahead of print]

Immunomodulatory role of megakaryocytes in the hematopoietic niche of myeloproliferative neoplasms

Xiaoxi Yang[1,2,*], Sandy Lee[3,*], Kyla Masarik[1], Tameena Ahmed[4], Lei Zheng[5], Huichun Zhan[1,6]

[1]Department of Medicine, Stony Brook School of Medicine, Stony Brook, NY
[2]Division of Rheumatology, Peking Union Medical College Hospital, Beijing, China
[3]The Graduate Program in Molecular & Cellular Biology, Stony Brook University, Stony Brook, NY
[4]Department of Pathology, Stony Brook University, Stony Brook, NY
[5]The Mays Cancer Center at the University of Texas Health, San Antonio, TX
[6]Medical Service, Northport VA Medical Center, Northport, NY

[*] X.Y. and S.L. contributed equally

Correspondence: Huichun Zhan, Division of Hematology-Oncology, Department of Medicine, Stony Brook University, Stony Brook, NY 11794; Northport VA Medical Center, 79 Middleville Road, Northport, NY 11768, USA.
E-mail: Huichun.Zhan@stonybrookmedicine.edu; Huichun.Zhan@va.gov
Phone: (631) 444-3901; Fax: (631) 544-5317

Word count for abstract: 227
Word count for text: 3509
Figure count: 6
Reference count: 59

Running title: Immunomodulatory Role of Megakaryocytes

ACKNOWLEDGEMENTS
We thank Dr. Kathleen Burns (Dana-Farber Cancer Institute, Harvard Medical School) for her valuable insights and discussions on the LINE-1 research.

FUNDING
This research was supported by the VA Merit Award BX003947 and BX005584 (H.Z.) and NIH R01 HL134970 and R01 CA266294 (H.Z.).

AUTHOR CONTRIBUTIONS
X.Y. and S.L. performed transgenic murine model experiments and data analysis; X.Y. also conducted patient sample studies; K.M. contributed to transgenic murine model studies and scRNAseq data analysis; T. Ahmed provided patient samples; L. Zheng provided scientific and technical support for immunology studies; H. Zhan designed and supervised the experiments, analyzed data, interpreted results, and wrote the manuscript. All authors read and approved the manuscript.

CONFLICT-OF-INTEREST DISCLOSURE
The authors declare no competing financial interests

DATA-SHARING STATEMENT
RNA sequencing data will be deposited in GEO data repository. Other data that support the findings of this study are available from the corresponding author upon reasonable request.

Abstract

Myeloproliferative neoplasms (MPNs) are clonal stem cell disorders characterized by dysregulated megakaryopoiesis and expansion of neoplastic hematopoietic stem cells (HSCs). Megakaryocytes (MKs) not only regulate HSC function but also shape immune responses within the marrow niche. Using an aging murine model of MPN with MK-restricted JAK2V617F expression, we investigated the immunomodulatory roles of mutant MKs. Compared to wild-type MKs, aged mutant MKs exhibit enhanced antigen uptake and MHC I presentation, secretion of pro-inflammatory cytokines (PF4, TGFβ, IL-1β), and induction of T cell dysregulation in the marrow niche. In chimeric murine models with co-existing wild-type and JAK2V617F mutant hematopoietic cells, enhanced MK immune activity correlates with mutant cell expansion and MPN development. Single-cell RNA sequencing revealed that aging amplifies JAK2V617F MK–driven immune remodeling. Notably, aged mutant MKs showed marked upregulation of *LINE-1* (long-interspersed element-1) retrotransposon transcripts alongside elevated innate immune sensors cyclic GMP−AMP synthase (cGAS) and stimulator of interferon genes (STING), implicating retrotransposon activity in niche inflammation. In human MPN marrow, immunohistochemistry detected LINE-1–encoded protein ORF1p in MKs from 12 of 13 MPN patients, but not in orthopedic controls (n=5). These findings identify MKs as active immune regulators in MPNs, with JAK2V617F mutation and aging synergizing to reprogram MKs into inflammatory, immune-modulatory niche cells. *LINE-1* activation emerges as a potential driver of chronic marrow inflammation and a targetable mechanism in clonal hematopoiesis and MPN progression.

Introduction

Megakaryocytes (MKs), traditionally recognized as the precursors of platelets, have emerged as key regulators of the hematopoietic stem cell (HSC) function. Through the production of cytokines, chemokines, and extracellular matrix components, MKs influence both steady-state and stress hematopoiesis[1-5]. Recent studies also suggest that MKs contribute to pathogen surveillance and immune regulation[6-11]. While abnormal megakaryopoiesis is a common feature of many hematologic malignancies[12-16], how diseased MKs alter their immunomodulatory function and impact HSC behavior in normal and neoplastic hematopoiesis remains poorly understood.

Myeloproliferative neoplasms (MPNs), including polycythemia vera (PV), essential thrombocythemia (ET), and primary myelofibrosis (PMF), are clonal stem cell disorders characterized by hematopoietic stem/progenitor cell (HSPC) expansion and an increased risk of transformation to acute leukemia. The acquired kinase mutation JAK2V617F plays a central role in these diseases[17, 18]. MK hyperplasia is a hallmark feature of MPNs, with advanced disease often associated with morphologically and functionally altered MKs, raising the possibility that diseased MKs contribute to disease progression[12, 14, 15, 19]. Both MPN incidence and leukemia transformation risk increase significantly with aging[17, 18], suggesting a strong interplay between JAK2V617F-driven hematopoiesis and age-related changes in the marrow microenvironment.

We previously established a MPN model in which JAK2V617F mutant MKs drive a myeloproliferative syndrome characterized by modest thrombocytosis, splenomegaly, increased marrow MKs, and expansion of wild-type HSCs compared to age-matched control mice[20]. Using competitive repopulation assays, we found that while HSCs from young mutant MK mice exhibited enhanced engraftment potential, 2-year-old JAK2V617F mutant MK mice displayed features of age-related HSC dysfunction — reduced engraftment, myeloid-skewed hematopoiesis with expansion of $CD41^+$ myeloid-biased HSCs, and decreased quiescence[21]. These findings suggest that JAK2V617F mutant MKs progressively impair wild-type HSC function with age. In the current study, we investigate how mutant MKs contribute to MPN development through immunomodulation. Given that chronic inflammation is a hallmark of MPN and is known to favor the expansion of JAK2V617F mutant over co-existing wild-type cells[22], we hypothesize that during aging, JAK2V617F mutant MKs acquire immune modulatory functions, drive marrow inflammation, and promote neoplastic clone expansion.

Methods

Experimental mice

All mouse experiments were performed according to protocols approved by the Institutional Animal Care and Use Committee at Stony Brook University. JAK2V617F Flip-Flop (FF1) mice (which carry a Cre- inducible human JAK2V617F gene driven by the human JAK2 promoter) were provided by Radek Skoda (University Hospital Basal, Switzerland). Pf4-Cre mice (which express Cre under the promoter of platelet factor 4; JAX stock #008535) were crossed with the FF1 mice to generate a transgenic mouse line with human JAK2V617F expression in the MK lineage ($Pf4^+FF1^+$). and Tie2-cre mice were obtained from Jackson Laboratory. All mice used were housed in a pathogen-free mouse facility at Stony Brook University. No randomization or blinding was used to allocate experimental groups.

Patient samples

Archived bone marrow biopsies from MPN patients and age-matched orthopedic surgery controls were obtained from Stony Brook University hospital. Sample collection and analysis were conducted under an Institutional Review Board-approved protocol. A detailed list of patient samples used in this study is provided in Figure 7.

Additional methods can be found in the supplemental Methods.

Results

JAK2V617F mutant MKs remodel the bone marrow immune microenvironment in $Pf4^+FF1^+$ mice during aging

To investigate the immunomodulatory functions of JAK2V617F mutant MKs *in vivo*, we crossed mice with a Cre-inducible human JAK2V617F transgene (FF1)[23] with the Pf4-cre mice, in which Cre recombinase is driven by the MK-specific platelet factor 4 promoter[24]. Although the Pf4-cre model has some limitations including its expression in other cell lineages, it has remained a gold standard for creating efficient MK-specific transgene expression[25]. Using rigorous and sensitive assays (e.g., expression of fluorescent reporter genes, expression

of the JAK2V617F transgene, functional analysis of JAK/STAT downstream signaling), we and others verified the specific transgene expression and/or activation in MKs, but not in HSCs[3, 20, 21, 26, 27]. Previously, we demonstrated that JAK2V617F mutant MKs drive a myeloproliferative syndrome characterized by thrombocytosis, splenomegaly, and expansion of hematopoietic stem/progenitor cells (HSPCs)[20]. We also showed that these mutant MKs accelerate HSC aging, leading to myeloid-skewed hematopoiesis, expansion of $CD41^+$ HSCs, and reduced engraftment, self-renewal, and differentiation capacity compared to age-matched controls[21]. Thus, Pf4-cre$^+$FF1$^+$ ($Pf4^+FF1^+$) mice provide a unique model to study the immunomodulatory functions of MKs and their effects on the marrow microenvironment of MPNs during aging.

Consistent with our previous reports[20, 21], $Pf4^+FF1^+$ mice developed an essential thrombocythemia phenotype, exhibiting modest neutrophilia and sustained thrombocytosis over a 2-year follow up (Figure 1A). In aged (2-year old) mice, flow cytometry revealed a marked increase in $CD3^+CD8^+$ T cells accompanied by a reduction in regulatory T (Treg) cells — changes not observed in young mice (Figure 1B-C). Despite the numeric increase, $CD8^+$ T cells from aged $Pf4^+FF1^+$ mice exhibited impaired cytotoxic function, as evidenced by reduced intracellular IFNγ levels (Figure 1D). Overall, both control and mutant mice exhibited an age-associated expansion of marrow $CD3^+$ T cells and a decline in Treg cells, with these changes being more pronounced in $Pf4^+FF1^+$ mice (Figure 1E). Collectively, these findings suggest that, in the context of aging, JAK2V617F mutant MKs can alter the bone marrow immune landscape. Previously, we demonstrated that the human JAK2 transgene is not expressed in HSCs from either young (6mo-old)[20] or old (2yr-old)[21] $Pf4^+FF1^+$ mice using sensitive reverse transcription polymerase chain reaction (RT-PCR) assays. In the present study, we further confirmed that the human JAK2 gene is not expressed in flow-sorted long-term HSCs ($Lin^-cKit^+Sca1^+CD150^+CD48^-$), short-term HSCs ($Lin^-cKit^+Sca1^+CD150^-CD48^-$), MPP2 ($Lin^-cKit^+Sca1^+CD150^+CD48^+$), and MPP3 ($Lin^-cKit^+Sca1^+CD150^-CD48^+$) populations[28, 29], as well as in sorted T cells ($CD45^+Gr1^-CD11b^-B220^-CD3^+$), B cells ($CD45^+Gr1^-CD11b^-B220^+CD3^-$), macrophages ($CD45^+Gr1^+CD11b^+F4/80^+$, and myeloid cells ($CD45^+Gr1^+CD11b^+F4/80^-$) from 2yr-old $Pf4^+FF1^+$ mice (Figure 1F). These findings confirm that the human JAK2 transgene is not expressed outside the MK lineage.

To investigate how JAK2V617F mutant MKs alter the marrow immune microenvironment, we performed single-cell RNA-seq (scRNAseq) on unfractionated marrow cells from young (4mo) and aged (1yr) $Pf4^+FF1^+$ and control mice (n=1 per group). Following data integration, doublet removal and quality control (see Methods), 47,730 cells were analyzed from 4 mice (9,800 – 15,678 cells per mouse). Unsupervised clustering of all the data identified 29 clusters of marrow cells, visualized by uniform manifold approximation and projection (UMAP). Cell identity was manually assigned to clusters based on the differential expression of known marker genes, identifying distinct immune and hematopoietic populations including neutrophil, monocyte-macrophage, T-NK cell, B cell, dendritic cell, granulocyte-monocyte progenitor, MK-HSPC, eosinophil-basophil-mast cell, and erythrocyte cell populations (Figure 2A). We performed an integrated cluster analysis of the mixed MK/HSPC population. HSPCs were identified by enriched expression of CD34, Flt3, and CD27, while MKs were characterized by high expression of Pf4, Gp9, Mpl, and vWF (Figure 2B). We did not detect any distinct “immune MK” populations with high Ccl3, Ccl4, Cd53, Lsp1, or Cxcr4 expression[11, 30-32], likely because our scRNAseq was performed on unfractionated marrow cells rather than MK-enriched samples.

Consistent with previous findings of decreased HSC proliferation in young $Pf4^+FF1^+$ mice but increased activity in aged $Pf4^+FF1^+$ mice[21, 33], gene sets associated with proliferation (e.g., MYC targets, G2/M checkpoint, E2F targets) were significantly upregulated in HSCs from aged $Pf4^+FF1^+$ mice compared to age-matched controls, contrasting with their expression patterns in young mice (Figure 2C). Gene set enrichment analysis (GSEA) of MKs revealed that immune response pathways (e.g., Interferon gamma response, Interferon alpha response, and TNFα signaling via NFκb) were significantly upregulated in aged $Pf4^+FF1^+$ mice, but not in young mice, reinforcing the idea that aging amplified mutant MK-driven immune modulation (Figure 2D). Beyond HSPCs and MKs, cell proliferation (e.g., MYC targets, G2/M checkpoint, E2F targets), inflammation and immune activation (e.g., PI3K AKT MTOR signaling, Reactive oxygen species pathway, IL6 JAK STAT3 signaling, Oxidative phosphorylation, TNFα signaling via NFκb, Interferon alpha response), and metabolic pathways (e.g., cholesterol homeostasis, fatty acid metabolism, glycolysis, MTORCS signaling) were highly upregulated in neutrophils and T cells in aged $Pf4^+FF1^+$ mice compared to age-matched controls, reflecting a pro-inflammatory marrow immune microenvironment (Figure 2E). In contrast, while cell proliferation pathways are significantly upregulated in monocytes and macrophages from aged $Pf4^+FF1^+$ mice, IL6/JAK/STAT3, TNFα/NFkB, interferon, and inflammatory response genes are notably downregulated, indicating a shift toward a less immune-active phenotype of these cells with aging (Supplementary Figure 1).

Taken together, these findings suggest that JAK2V617F mutant MKs drive chronic inflammation and immune activation in the marrow, accompanied by skewed T cell populations (Figure 1B-C), impaired T cell function (Figure 1D), and an immune-suppressive monocyte phenotype (Figure 2F).

The modulatory functions of JAK2V617F mutant MKs in both innate and adaptive immunity

We assessed the ability of JAK2V617F mutant MKs to process exogenous protein antigens[8, 10]. Marrow MKs from aged wild-type and $Pf4^+FF1^+$ mice were cultured with 200ug/ml DQ-Ovalbumin (DQ-Ova) and cell fluorescence was measured by flow cytometry and fluorescence microscope (Figure 3A; Supplementary Figure 2A) 2hr later as a measure of Ova processing (DQ-Ova fluorescence is only activated upon cellular uptake and proteolytic cleavage). Antigen presentation on MHC I was evaluated using an anti-MHC class I-Ova antibody. JAK2V617F mutant MKs from aged $Pf4^+FF1^+$ mice showed enhanced Ova antigen uptake, processing, and presentation on MHC I compared to wild-type MKs from aged control mice.

To validate murine findings in human cells, we assessed the antigen-processing ability of JAK2V617F mutant human MKs. For this study, we obtained a JAK2V617F homozygous mutant induced pluripotent stem (iPS) cell line derived from a MPN patient (PVB1.4) and a JAK2 wild-type iPS cell line derived from a healthy donor (BC1)[34]. Their genotypes and JAK2 gene expression were confirmed by a nested allele-specific PCR assay[35] (Supplementary Figure 3A-C). These iPS cells can be differentiated into $CD34^+CD45^+$ hematopoietic progenitors using the spin-embryoid body method, harvested after 2-3 weeks, and further differentiated into $CD41^+CD42^+$ mature MKs[36-38] (Supplementary Figure 3D-E). Wild-type (BC1-derived) or JAK2V617F mutant (PVB1.4-derived) MKs were cultured with 200ug/ml Ovalbumin-Alexa Fluor 647 for 2 hours at 37ºC. Consistent with our findings in murine MKs (Figure 3A), JAK2V617F mutant human MKs also show increased Ova uptake and MHC class I presentation compared to wild-type MKs (Figure 3B; Supplementary Figure 2A), validating the mouse observations.

To determine whether MKs interact with T cells in an antigen-specific manner, we used OT-I and OT-II transgenic mice, which recognize MHC I-restricted Ova257-264 and MHC II-restricted Ova323-339 peptides, respectively[39, 40]. Wild-type mice were treated with a single dose of 25ug Ova257-264, Ova323-339, or PBS via intraperitoneal injection. One hour later, marrow MKs were isolated and co-cultured with naïve OT-I $CD8^+$ or OT-II $CD4^+$ T cells. IFNγ expression and cell proliferation (by carboxyfluorescein succinimidyl ester, or CFSE label dilution) were assessed. Ova257-264-loaded marrow MKs significantly enhanced CD8+ T cell proliferation and transiently increased IFNγ production, peaking at Day 2. In contrast, Ova323-339-loaded marrow MKs had no effect on $CD4^+$ T cells (Figure 3C). To confirm that Ova257-264-stimulated MKs directly activate $CD8^+$ T cells, wild-type marrow MKs were pulsed with Ova257-264 *in vitro* (2.5ug/ml, 2 hours at 37°C) before co-culture with OT-I splenic $CD8^+$ T cells. A mouse IFNγ Enzyme-linked immunospot (ELISpot) assay revealed a significant increase in IFNγ-secreting $CD8^+$ T cells, consistent with *in vivo* findings (Figure 3D). We observed no significant differences in T cell proliferation or activation between wild-type and JAK2V617F mutant MKs (data not shown), suggesting that both MK types can engage T cells in an antigen-specific manner, although the potency of Ova257-264 may mask their functional differences.

An important function of innate immunity is the production of cytokines to modulate immune responses. To assess their cytokine profiles, we performed targeted cytokine arrays (Abcam®, Cat. 133995) on wild-type and JAK2V617F MKs isolated from young and old mice. Marrow MKs from 2-4 mice per group were pooled to reduce the effects of individual sample variability. In aged $Pf4^+FF1^+$ mice, mutant MKs exhibited elevated expression of multiple inflammatory cytokines compared to wild-type MKs from age-matched controls (Supplementary Figure 2B). Next, we analyzed marrow plasma (collected by flushing each murine femur with 0.5ml PBS followed by centrifugation at 2,000g for 15min) using ELISA. This revealed significantly increased levels of PF4 (Platelet factor 4), TGFβ (Transforming growth factor beta), and IL1β (Interleukin-1 beta) in aged $Pf4^+FF1^+$ mice compared to controls, whereas no difference was observed in young mice (Figure 3E). MKs are the primary source of PF4 in the marrow[4], and its plasma levels are known to be elevated in many MPN patients[41, 42]. PF4 has been implicated in immune cell recruitment[43], monocyte differentiation[44, 45], and $CD8^+$ T cell inhibition[44, 46]. Therefore, PF4 upregulation may contribute to immune dysfunction driven by JAK2V617F mutant MKs.

Overall, JAK2V617F mutant MKs upregulate inflammatory and immune-regulatory genes, produce pro-inflammatory cytokines, present antigens, and modulate T cell functions — all of which may contribute to the inflammatory marrow niche that characterizes MPNs and promotes expansion of mutant over wild-type cells[22].

Increased inflammatory and immunomodulatory gene expression in MKs correlates with higher mutant cell burden in a murine model with co-existing wild-type and JAK2V617F mutant cells

To test whether this heightened immune modulatory MK signature is linked to MPN disease progression, we generated chimeric murine models harboring both wild-type and JAK2V617F mutant hematopoietic cells at varying ratios to model MPN mutant cell expansion. We used the Tie2-cre^{+}FF1^{+} murine model we previously established in which human JAK2V617F is expressed in all hematopoietic cells[47-49]. In brief, lethally irradiated wild-type mice (CD45.1) were transplanted with both wild-type marrow cells (isolated from CD45.1 wild-type mice) and JAK2V617F mutant marrow cells (isolated from CD45.2 Tie2-cre^{+}FF1^{+} mice) mixed at ratios of 100:0, 90:10, 10:90. These chimeric mice exhibited a “dose-dependent” MPN phenotype, with those receiving a higher proportion (90%) mutant donor cells developing leukocytosis, thrombocytosis, and an increased marrow Lin^{-}cKit^{+}Sca1^{+} (LSKs) and Lin^{-}cKit^{+}Sca1^{+}CD150^{+}CD48^{-} (HSCs) 16 weeks post-transplantation, while those receiving a lower proportion (10%) of mutant donor cells remained asymptomatic throughout the 4-month follow-up period (Figure 4A).

We conducted scRNAseq analysis on unfractionated marrow cells from three chimeric mice (A, B, and C), characterized by varying mutant cell burdens and distinct hematologic phenotypes at different time points post-transplantation (Figure 4B). After quality filtering, a total of 15,403 cells from three mice were included in the analysis (Figure 4C). MKs were identified by expression of established marker genes, including Itga2b, Pf4, Gp9, vWF, and MPL. Comparative analysis of gene expression profiles revealed significant enrichment of cell proliferation, inflammation, and immune activation gene sets in MKs from the high mutant burden MPN mouse (Mouse C) compared to MKs from a low mutant burden, non-MPN mouse (Mouse A). Similarly, MKs from Mouse C showed the same enrichment when compared to MKs from a comparable mutant burden, non-MPN mouse (Mouse B) (Figure 4D-E). These findings suggest that heightened immunomodulatory signatures in MKs are associated with mutant cell burden and may contribute to MPN development (mouse C vs. mouse A) and that the immunomodulatory functions of mutant MKs are not solely attributable to the presence of the JAK2V617F mutation alone (mouse C vs. mouse B). In contrast, angiogenesis and oxidative phosphorylation pathways were significantly enriched in MKs from Mouse B compared to MKs from Mouse A, indicating a metabolically active and proangiogenic state in MKs from mice with high mutant burden but no MPN blood phenotype (Supplementary Figure 4).

Elevated LINE-1 transcription in bone marrow MKs in MPN murine models.

Half of the human genome consists of transposable elements, with LINE-1 (long-interspersed element-1) being the only protein-coding transposon that remains active in humans[50]. While LINE-1 reverse transcriptase activity has been detected in human and mouse platelets[51], little is known about its expression in MKs. Since LINE-1 activation is linked to DNA replication and cell cycling[52], and MKs undergo endomitosis — a unique form of cell cycling during which MKs undergo multiple rounds of DNA synthesis without cell division[53] — it is likely that LINE-1 activity increases in MKs with aging.

Full-length LINE-1 elements in mice span ~7kb, containing a 5’ UTR, two open reading frames ORF1 and ORF2, and a 3’ UTR with a poly(A) tail. RT-qPCR using multiple primer pairs targeting active LINE-1 families[54] revealed a significant increase in 5’UTR, ORF1, ORF2, and 3’UTR transcripts in mutant MKs from aged mice, but not young mice (Figure 5A). Such trend was not observed in other marrow cell populations including CD3^{+} T cells, B220^{+} B cells, CD11b^{+} myeloid cells, or Lin^{-}cKit^{+}Sca1^{+} HSPCs (Figure 5B). Treating marrow MKs from aged control and Pf4^{+}FF1^{+} mice with lamivudine (25uM for 24hrs), a reverse transcriptase inhibitor used to suppress HIV replication, significantly reduced LINE-1 transcripts in mutant MKs (Figure 5C). Although this is likely an indirect effect of reverse transcription inhibition, it suggests that retrotransposition contributes to the elevated LINE-1 RNA levels observed in JAK2V617F mutant MKs. Given LINE-1’s role in aging and innate immunity, its upregulation in aged mutant MKs may drive innate immune activation and inflammatory remodeling of the marrow[54-57]. Consistent with this, the innate immune sensors cyclic GMP−AMP synthase (cGAS) and stimulator of interferon genes (STING), which induce interferon and interferon-regulated genes[50], are upregulated in JAK2V617F mutant MKs from aged Pf4^{+}FF1^{+} mice (Figure 5D).

LINE-1 ORF1p protein expression in marrow MKs of MPN patients

Finally, we assessed LINE-1 expression in marrow biopsies from MPN patients (n=13, average age 71yr) and age-matched controls from orthopedic surgery patients (4 hip marrow samples and 1 rib marrow samples; average age 71yr) using immunohistochemistry (IHC) for CD41 and ORF1p. ORF1p staining was validated in adult testis tissue, known to low ORF1p expression[58], and MKs were identified based on morphology and

CD41 positivity (Figure 6A). No ORF1p protein was detected in any of the five control marrow samples. In contrast, ORF1p expression was observed in marrow MKs in 12 out of 13 MPN patients, with varying levels of positivity (Figure 6B). Within individual MPN patients, both ORF1p-positive and ORF1p-negative MKs co-existed, with 40-100% MKs expressing ORF1p in affected patients (Figure 6C). Notably, while ORF1p expression was largely restricted to MKs, diffuse ORF1p expression in non-MK marrow cells was observed in two patients with advanced disease — one transitioning from PV to myelodysplastic syndrome (MDS) (patient #SL025) and another with accelerated-phase post-PV myelofibrosis (MF) (patient #SL046) (Figure 6D). These findings suggest that LINE-1 activation is a hallmark of MPN marrow MKs, with its expression increasing in advanced disease stages. The presence of ORF1p in non-MK marrow cells in progressive MPN cases further raises the possibility that LINE-1 activation extends beyond MKs during disease evolution, potentially contributing to neoplastic clonal expansion.

Discussion

MKs, long recognized for their role in platelet production, are increasingly understood as key regulators of the hematopoietic and immune microenvironment. By producing inflammatory cytokines and immune mediators, MKs actively participate in pathogen surveillance and immune responses in tissue microenvironment[6-11, 59]. However, how diseased MKs alter these functions to influence HSC behavior in neoplastic hematopoiesis remains unclear. Our findings suggest that JAK2V617F mutant MKs may act as potent immunomodulators, contributing to the reprogramming of the marrow immune microenvironment and potentially promoting disease progression in MPNs. Compared to wild-type MKs, mutant MKs exhibit heightened inflammation and innate immune activation, including increased antigen presentation, elevated pro-inflammatory cytokines (PF4, TGFβ, IL1β), skewed T cell populations, and impaired T cell functions in the JAK2V617F-bearing MK niche *in vivo*. These changes are further amplified by aging, a major risk factor for MPN progression. To determine the impact of MK-driven immune dysregulation on MPN evolution, we developed a chimeric murine model with co-existing wild-type and JAK2V617F mutant HSCs, mimicking the competitive dynamics observed in MPN patients. Our results reveal that enhanced MK immunomodulatory function is linked to JAK2V617F mutant cell expansion, underscoring MKs' role as key drivers of clonal hematopoiesis. These findings were further validated in human cells using an MPN patient-derived iPS cell line model, which allowed us to confirm increased antigen processing and presentation in JAK2V617F mutant MKs compared to wild-type MKs in a genetically controlled system.

Approximately half of the human genome is composed of transposable elements, with LINE-1 being the only protein-coding transposon still active in humans[50]. As LINE-1 replicates itself using RNA intermediates via retrotransposition, LINE-1-derived endogenous nucleic acids can act as danger signals to trigger the innate immune response via pattern recognition receptors, leading to immune cell activation and the production of inflammatory cytokines[60]. LINE-1 retrotransposition activity peaks during cell cycling and DNA replication[52]. MKs, which undergo endomitosis and accumulate large amounts of DNA and RNA, may therefore be particularly vulnerable to LINE-1 reactivation. However, the role of LINE-1 in MKs has been largely unexplored. Here, we show that LINE-1 transcripts and the innate immune sensors cGAS and STING are significantly upregulated in aged JAK2V617F mutant MKs in a murine model of MPN (Figure 5). This finding is corroborated by detection of LINE-1–encoded ORF1p protein in marrow MKs from 13 of 14 MPN patients, but not in age-matched controls undergoing orthopedic surgery (Figure 6). Given that LINE-1 activation is a known driver of innate immune activation and is implicated in aging-related inflammation[54-57], our findings suggest that elevated LINE-1 expression in diseased MKs may contribute to the inflammatory marrow microenvironment characteristic of MPNs.

While chronic inflammation is a well-established driver of HSC stress and aging-associated hematological disorders, the specific niche cells responsible for inflammatory cytokine production remain poorly defined. Our findings suggest that MKs play an important role in regulating niche inflammation in MPNs during aging, and they can influence both innate and adaptive immunity to shape a marrow microenvironment that favors neoplastic HSC expansion over wild-type hematopoiesis. The translational significance of these findings extends beyond MPNs. Abnormal megakaryopoiesis is a common feature of many hematologic malignancies[12-16], and aging-associated clonal hematopoiesis is increasingly recognized as a risk factor for cardiovascular disease, immune dysregulation, and cancer[61]. Our study highlights a broader role for MK-driven inflammation in shaping both the marrow and systemic immune landscape, with potential implications for developing novel therapeutic strategies targeting inflammatory and immune pathways activated in mutant MKs. Several important questions remain. For instance, how does JAK2V617F promote LINE-1 activation in MKs? Does MK-

driven inflammation cause or accelerate MPN disease progression, or is it merely a consequence of clonal expansion? Answering these questions will be critical for establishing MKs as key regulators of marrow inflammation and immune modulation, and for developing targeted therapies that disrupt the vicious cycle of mutant MK-driven inflammation, immune dysfunction, and clonal expansion.

REFERENCES

1. Zhao M, Ross JT, Itkin T, et al. FGF signaling facilitates postinjury recovery of mouse hematopoietic system. Blood. 2012;120(9):1831-1842.
2. Heazlewood SY, Neaves RJ, Williams B, Haylock DN, Adams TE, Nilsson SK. Megakaryocytes co-localise with hemopoietic stem cells and release cytokines that up-regulate stem cell proliferation. Stem Cell Res. 2013;11(2):782-792.
3. Zhao M, Perry JM, Marshall H, et al. Megakaryocytes maintain homeostatic quiescence and promote post-injury regeneration of hematopoietic stem cells. Nat Med. 2014;20(11):1321-1326.
4. Bruns I, Lucas D, Pinho S, et al. Megakaryocytes regulate hematopoietic stem cell quiescence through CXCL4 secretion. Nat Med. 2014;20(11):1315-1320.
5. Zhan H, Kaushansky K. Megakaryocytes as the Regulator of the Hematopoietic Vascular Niche. Front Oncol. 2022;12:912060.
6. Kang HK, Chiang MY, Ecklund D, Zhang L, Ramsey-Goldman R, Datta SK. Megakaryocyte progenitors are the main APCs inducing Th17 response to lupus autoantigens and foreign antigens. J Immunol. 2012;188(12):5970-5980.
7. Finkielsztein A, Schlinker AC, Zhang L, Miller WM, Datta SK. Human megakaryocyte progenitors derived from hematopoietic stem cells of normal individuals are MHC class II-expressing professional APC that enhance Th17 and Th1/Th17 responses. Immunol Lett. 2015;163(1):84-95.
8. Zufferey A, Speck ER, Machlus KR, et al. Mature murine megakaryocytes present antigen-MHC class I molecules to T cells and transfer them to platelets. Blood Adv. 2017;1(20):1773-1785.
9. Campbell RA, Schwertz H, Hottz ED, et al. Human megakaryocytes possess intrinsic antiviral immunity through regulated induction of IFITM3. Blood. 2019;133(19):2013-2026.
10. Pariser DN, Hilt ZT, Ture SK, et al. Lung megakaryocytes are immune modulatory cells. J Clin Invest. 2021;131(1):e137377.
11. Wang J, Xie J, Wang D, et al. CXCR4(high) megakaryocytes regulate host-defense immunity against bacterial pathogens. Elife. 2022;11:e78662.
12. Ciurea SO, Merchant D, Mahmud N, et al. Pivotal contributions of megakaryocytes to the biology of idiopathic myelofibrosis. Blood. 2007;110(3):986-993.
13. Geissler D, Zwierzina H, Pechlaner C, et al. Abnormal megakaryopoiesis in patients with myelodysplastic syndromes: analysis of cellular and humoral defects. Br J Haematol. 1989;73(1):29-35.
14. Malherbe JA, Fuller KA, Arshad A, et al. Megakaryocytic hyperplasia in myeloproliferative neoplasms is driven by disordered proliferative, apoptotic and epigenetic mechanisms. J Clin Pathol. 2016;69(2):155-163.
15. Melo-Cardenas J, Migliaccio AR, Crispino JD. The Role of Megakaryocytes in Myelofibrosis. Hematol Oncol Clin North Am. 2021;35(2):191-203.
16. Wen Q, Goldenson B, Crispino JD. Normal and malignant megakaryopoiesis. Expert Rev Mol Med. 2011;13:e32.
17. Spivak JL. Myeloproliferative Neoplasms. N Engl J Med. 2017;376(22):2168-2181.
18. Nangalia J, Green AR. Myeloproliferative neoplasms: from origins to outcomes. Hematology Am Soc Hematol Educ Program. 2017;2017(1):470-479.
19. Guo BB, Allcock RJ, Mirzai B, et al. Megakaryocytes in Myeloproliferative Neoplasms Have Unique Somatic Mutations. Am J Pathol. 2017;187(7):1512-1522.
20. Zhan H, Ma Y, Lin CH, Kaushansky K. JAK2(V617F)-mutant megakaryocytes contribute to hematopoietic stem/progenitor cell expansion in a model of murine myeloproliferation. Leukemia. 2016;30(12):2332-2341.

21. Lee S, Wong H, Castiglione M, Murphy M, Kaushansky K, Zhan H. JAK2V617F Mutant Megakaryocytes Contribute to Hematopoietic Aging in a Murine Model of Myeloproliferative Neoplasm. Stem Cells. 2022;40(4):359-370.
22. Mendez Luque LF, Blackmon AL, Ramanathan G, Fleischman AG. Key Role of Inflammation in Myeloproliferative Neoplasms: Instigator of Disease Initiation, Progression. and Symptoms. Curr Hematol Malig Rep. 2019;14(3):145-153.
23. Tiedt R, Hao-Shen H, Sobas MA, et al. Ratio of mutant JAK2-V617F to wild-type Jak2 determines the MPD phenotypes in transgenic mice. Blood. 2008;111(8):3931-3940.
24. Tiedt R, Schomber T, Hao-Shen H, Skoda RC. Pf4-Cre transgenic mice allow the generation of lineage-restricted gene knockouts for studying megakaryocyte and platelet function in vivo. Blood. 2007;109(4):1503-1506.
25. Gollomp K, Poncz M. Gp1ba-Cre or Pf4-Cre: pick your poison. Blood. 2019;133(4):287-288.
26. Ng AP, Kauppi M, Metcalf D, et al. Mpl expression on megakaryocytes and platelets is dispensable for thrombopoiesis but essential to prevent myeloproliferation. Proc Natl Acad Sci U S A. 2014;111(16):5884-5889.
27. Woods B, Chen W, Chiu S, et al. Activation of JAK/STAT Signaling in Megakaryocytes Sustains Myeloproliferation In Vivo. Clin Cancer Res. 2019;25(19):5901-5912.
28. Pietras EM, Reynaud D, Kang YA, et al. Functionally Distinct Subsets of Lineage-Biased Multipotent Progenitors Control Blood Production in Normal and Regenerative Conditions. Cell Stem Cell. 2015;17(1):35-46.
29. Oguro H, Ding L, Morrison SJ. SLAM family markers resolve functionally distinct subpopulations of hematopoietic stem cells and multipotent progenitors. Cell Stem Cell. 2013;13(1):102-116.
30. Sun S, Jin C, Si J, et al. Single-cell analysis of ploidy and the transcriptome reveals functional and spatial divergency in murine megakaryopoiesis. Blood. 2021;138(14):1211-1224.
31. Liu C, Wu D, Xia M, et al. Characterization of Cellular Heterogeneity and an Immune Subpopulation of Human Megakaryocytes. Adv Sci (Weinh). 2021;8(15):e2100921.
32. Li JJ, Liu J, Li YE, et al. Differentiation route determines the functional outputs of adult megakaryopoiesis. Immunity. 2024;57(3):478-494.e476.
33. Zhang Y, Lin CHS, Kaushansky K, Zhan H. JAK2V617F Megakaryocytes Promote Hematopoietic Stem/Progenitor Cell Expansion in Mice Through Thrombopoietin/MPL Signaling. Stem Cells. 2018;36(11):1676-1684.
34. Ye Z, Liu CF, Lanikova L, et al. Differential sensitivity to JAK inhibitory drugs by isogenic human erythroblasts and hematopoietic progenitors generated from patient-specific induced pluripotent stem cells. Stem Cells. 2014;32(1):269-278.
35. Lu M, Wang X, Li Y, et al. Combination treatment in vitro with Nutlin, a small-molecule antagonist of MDM2, and pegylated interferon-alpha 2a specifically targets JAK2V617F-positive polycythemia vera cells. Blood. 2012;120(15):3098-3105.
36. Liu Y, Wang Y, Gao Y, et al. Efficient generation of megakaryocytes from human induced pluripotent stem cells using food and drug administration-approved pharmacological reagents. Stem Cells Transl Med. 2015;4(4):309-319.
37. Ye Z, Zhan H, Mali P, et al. Human-induced pluripotent stem cells from blood cells of healthy donors and patients with acquired blood disorders. Blood. 2009;114(27):5473-5480.
38. Li Y, Jin C, Bai H, et al. Human NOTCH4 is a key target of RUNX1 in megakaryocytic differentiation. Blood. 2018;131(2):191-201.
39. Hogquist KA, Jameson SC, Heath WR, Howard JL, Bevan MJ, Carbone FR. T cell receptor antagonist peptides induce positive selection. Cell. 1994;76(1):17-27.
40. Barnden MJ, Allison J, Heath WR, Carbone FR. Defective TCR expression in transgenic mice constructed using cDNA-based alpha- and beta-chain genes under the control of heterologous regulatory elements. Immunol Cell Biol. 1998;76(1):34-40.

41. Burstein SA, Malpass TW, Yee E, et al. Platelet factor-4 excretion in myeloproliferative disease: implications for the aetiology of myelofibrosis. Br J Haematol. 1984;57(3):383-392.
42. Capitanio D, Calledda FR, Abbonante V, et al. Proteomic screening identifies PF4/Cxcl4 as a critical driver of myelofibrosis. Leukemia. 2024;38(9):1971-1984.
43. Gray AL, Karlsson R, Roberts ARE, et al. Chemokine CXCL4 interactions with extracellular matrix proteoglycans mediate widespread immune cell recruitment independent of chemokine receptors. Cell Rep. 2023;42(1):111930.
44. Joseph R, Soundararajan R, Vasaikar S, et al. CD8(+) T cells inhibit metastasis and CXCL4 regulates its function. Br J Cancer. 2021;125(2):176-189.
45. Scheuerer B, Ernst M, Durrbaum-Landmann I, et al. The CXC-chemokine platelet factor 4 promotes monocyte survival and induces monocyte differentiation into macrophages. Blood. 2000;95(4):1158-1166.
46. Fleischer J, Grage-Griebenow E, Kasper B, et al. Platelet factor 4 inhibits proliferation and cytokine release of activated human T cells. J Immunol. 2002;169(2):770-777.
47. Zhan H, Lin CHS, Segal Y, Kaushansky K. The JAK2V617F-bearing vascular niche promotes clonal expansion in myeloproliferative neoplasms. Leukemia. 2018;32(2):462-469.
48. Lin CH, Kaushansky K, Zhan H. JAK2V617F-mutant vascular niche contributes to JAK2V617F clonal expansion in myeloproliferative neoplasms. Blood Cells Mol Dis. 2016;62:42-48.
49. Lin CHS, Zhang Y, Kaushansky K, Zhan H. JAK2V617F-bearing vascular niche enhances malignant hematopoietic regeneration following radiation injury. Haematologica. 2018;103(7):1160-1168.
50. Mendez-Dorantes C, Burns KH. LINE-1 retrotransposition and its deregulation in cancers: implications for therapeutic opportunities. Genes Dev. 2023;37(21-24):948-967.
51. Schwertz H, Rowley JW, Schumann GG, et al. Endogenous LINE-1 (Long Interspersed Nuclear Element-1) Reverse Transcriptase Activity in Platelets Controls Translational Events Through RNA-DNA Hybrids. Arterioscler Thromb Vasc Biol. 2018;38(4):801-815.
52. Mita P, Wudzinska A, Sun X, et al. LINE-1 protein localization and functional dynamics during the cell cycle. Elife. 2018;7:e30058.
53. Ravid K, Lu J, Zimmet JM, Jones MR. Roads to polyploidy: the megakaryocyte example. J Cell Physiol. 2002;190(1):7-20.
54. De Cecco M, Ito T, Petrashen AP, et al. L1 drives IFN in senescent cells and promotes age-associated inflammation. Nature. 2019;566(7742):73-78.
55. Simon M, Van Meter M, Ablaeva J, et al. LINE1 Derepression in Aged Wild-Type and SIRT6-Deficient Mice Drives Inflammation. Cell Metab. 2019;29(4):871-885.e875.
56. Gorbunova V, Seluanov A, Mita P, et al. The role of retrotransposable elements in ageing and age-associated diseases. Nature. 2021;596(7870):43-53.
57. Burns KH. Transposable elements in cancer. Nat Rev Cancer. 2017;17(7):415-424.
58. Rodic N, Sharma R, Sharma R, et al. Long interspersed element-1 protein expression is a hallmark of many human cancers. Am J Pathol. 2014;184(5):1280-1286.
59. Koupenova M, Livada AC, Morrell CN. Platelet and Megakaryocyte Roles in Innate and Adaptive Immunity. Circ Res. 2022;130(2):288-308.
60. Hartmann G. Nucleic Acid Immunity. Adv Immunol. 2017;133:121-169.
61. Jaiswal S, Ebert BL. Clonal hematopoiesis in human aging and disease. Science. 2019;366(6465):eaan4673.

Figure 1. Inflammatory and immune activation signatures in JAK2V617F mutant MKs linked to skewed marrow T cell populations during aging of $Pf4^+FF1^+$ mice**.** (**A**) Peripheral blood cell counts of $Pf4^+FF1^+$ (black line) and Pf4-cre control mice (dotted line) (n=10-23 mice in each group). (**B-C**) Frequency of bone marrow T cells ($CD3^+CD4^+$ helper T cells, $CD3^+CD8^+$ cytotoxic T cells, and $CD3^+CD4^+CD25^+FoxP3^+$ regulatory T cells), B cells ($CD3^-B220^+$), myeloid-derived suppressor cells or MDSCs (both $CD11b^+Ly6C^{high}Ly6G^-$ M-MDSCs and $CD11b^+Ly6C^{low}Ly6G^+$ PMN-MDSCs) in young (C) and old (D) Pf4-Cre control (grey) and $Pf4^+FF1^+$ (black) mice (young: n=5-11 mice in each group; old: n=3-10 mice in each group). (**D**) Flow cytometry quantification of intracellular IFN-γ protein levels in bone marrow $CD8^+$ T cells (n = 4-5 mice per group). (**E**) Overall comparison of marrow $CD3^+$ T cells and Treg cells in control and $Pf4^+FF1^+$ mice across aging (n=3-6 per group). (**F**) As determined by RT-PCR, human JAK2 gene was expressed in MKs, but not in long-term HSCs, short-term HSCs, MPP2, MPP3, T, B, macrophages, or myeloid cells isolated by flow cytometry from the bone marrow of two aged $Pf4^+FF1^+$ mice. ($*p < 0.05$; $***p < 0.001$)

Figure 2. scRNAseq analysis of marrow cells from young and aged $Pf4^+FF1^+$ mice. (**A**) Uniform manifold approximation and projection (UMAP) plot of unfractionated marrow cells, with key markers used to infer cell identity listed. (**B**) UMAP visualization of the MK/HSPC population, with key markers used for cell identity listed. (**C-D**) GSEA analysis of HSPCs (C) and MKs (D) from young (left) and old (right) mice. (**E**) Gene sets associated with cell proliferation (green), inflammation and immune activation (red), and metabolism (blue) in neutrophils and T cells from both young and old $Pf4^+FF1^+$ mice, each compared with age-matched controls.

Figure 3. The immunomodulatory functions of JAK2V617F mutant MKs. (**A**) Representative flow cytometry analysis (left) and fluorescence microscope images (right) showing wild-type and JAK2V617F mutant MKs processing DQ-Ova (green fluorescence) and presenting Ova peptide antigen on MHC I molecules (red fluorescence). Data are from one of three independent experiments that gave similar results. (**B**) Representative flow cytometry analysis (left) and fluorescence microscope images (right) of wild-type and JAK2V617F mutant iPS-derived human MKs uptake Ova (purple fluorescence) and present Ova peptide antigen on MHC I molecules (red fluorescence). Magnification: 1000x. (**C**) OT-I $CD8^+$ T cell and OT-II $CD4^+$ T cell proliferation and IFNγ expression following co-culture with marrow MKs from Ova-treated mice. Data are from one of two independent experiments that gave similar results. (**D**) IFNγ ELISpot assays showing OT-I $CD8^+$ T cell activation after co-culture with Ova257-284 pulsed MKs. Data are from one of three independent experiments that gave similar results. (**E**) Protein levels of PF4, TGFβ, and IL1β in marrow plasma from young and old $Pf4^+FF1^+$ mice and aged-matched controls (n=3-7 mice per group). (* $p < 0.05$; ** $p < 0.01$; *** $p < 0.001$; **** $p < 0.0001$)

Figure 4. Augmented inflammatory and immunomodulatory gene expression in MKs is associated with mutant cell expansion in MPN. (**A**) Peripheral blood WBC and platelet counts, marrow LSK and HSC numbers of the chimeric mice with varying mutant cell burdens (n=6-8 mice in each group). (**B**) Mice selected for scRNAseq analysis. (**C**) Uniform manifold approximation and projection (UMAP) plot showing cell clusters from unfractionated marrow cells. (**D**) Top gene sets significantly enriched in mouse C (90% mutant) MKs compared to mouse A (10% mutant) MKs. (**E**) Top gene sets significantly enriched in mouse C (90% mutant, positive MPN phenotype) MKs compared to mouse B (90% mutant, no MPN phenotype) MKs. ($*p < 0.05$; $**p < 0.01$; $***p < 0.001$)

Figure 5. Elevated LINE-1 expression in JAK2V617F mutant MKs during aging. (**A**) LINE-1 RNA levels measured using primers specific to the 5' UTR, ORF1, ORF2, and 3' UTR. The transcript levels are shown as fold changes relative to their expression levels in MKs from young control mice (n=3-4 mice in each group). (**B**) LINE-1 ORF1 (top) and ORF2 (bottom) expression in bone marrow T cells, B cells, myeloid cells, and $Lin^-cKit^+Sca1^+$ stem/progenitor cells isolated from young and aged mice, isolated by flow sorting. Each group represents pooled samples from two mice. (**C**) ORF1 and ORF2 RNA levels in control and JAK2V617F mutant

marrow MKs after lamivudine treatment. (**D**) cGAS and STING gene expression shown as fold change relative to their expression levels in MKs from young control mice (n=3-4 mice in each group). (∗p < 0.05; ∗∗p < 0.01; ∗∗∗p < 0.001; ∗∗∗∗p < 0.001)

Figure 6. LINE-1 ORF1p protein expression in marrow MKs from MPN patients. (**A**) Representative images of ORF1p-positive staining in a histologically normal adult testis (left) and CD41 staining in normal bone marrow (right). (**B**) ORF1p protein expression in marrow biopsies from a representative control patient and three MPN patients with low, moderate, and strong ORF1p expression. (**C**) Summary of gender, age, MPN diagnosis, and ORF1p-positive MK (%) in the thirteen MPN patients analyzed. (**D**) Diffuse ORF1p expression in the marrow of two MPN patients with disease progression. All images were captured at 400x magnification.

Figure 1

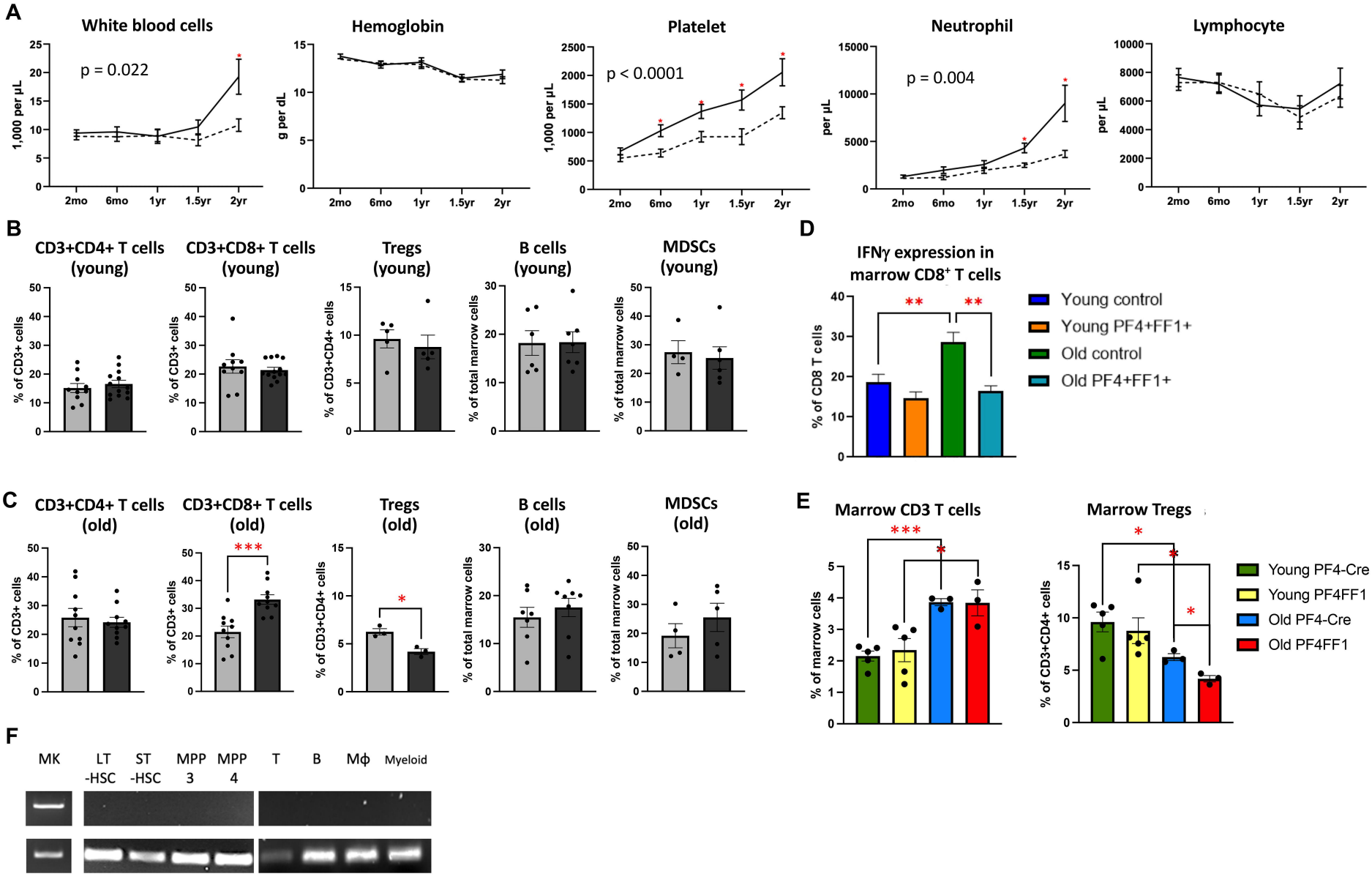
A
White blood cells
p = 0.022
1,000 per µL
Hemoglobin
g per dL
Platelet
p < 0.0001
1,000 per µL
Neutrophil
p = 0.004
per µL
Lymphocyte
per µL
2mo
6mo
1yr
1.5yr
2yr
B
CD3+CD4+ T cells (young)
CD3+CD8+ T cells (young)
Tregs (young)
B cells (young)
MDSCs (young)
% of CD3+ cells
% of CD3+CD4+ cells
% of total marrow cells
C
CD3+CD4+ T cells (old)
CD3+CD8+ T cells (old)
Tregs (old)
B cells (old)
MDSCs (old)
D
IFNγ expression in marrow CD8+ T cells
% of CD8 T cells
Young control
Young PF4+FF1+
Old control
Old PF4+FF1+
E
Marrow CD3 T cells
% of marrow cells
Marrow Tregs
% of CD3+CD4+ cells
Young PF4-Cre
Young PF4FF1
Old PF4-Cre
Old PF4FF1
F
MK
LT -HSC
ST -HSC
MPP 3
MPP 4
T
B
Mϕ
Myeloid

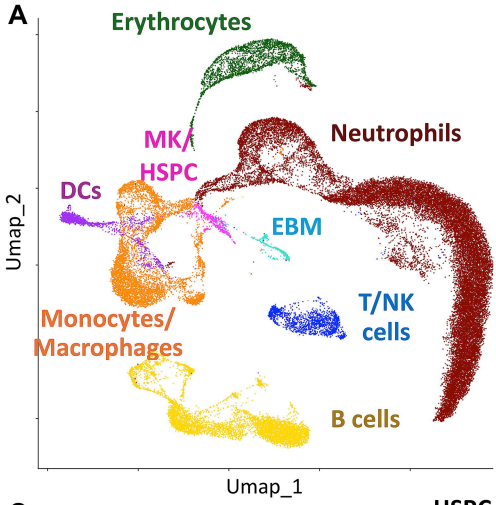

Neutrophils:
S100a8, S100a9, Ly6G
Monocytes-Macrophages:
Ccr2, Csf1r
B cells:
Cd79a
T cells-NK cells:
Cd3d, Ncr1
Dendritic cells (DCs):
Siglech
MK-HSC:
Itga2b, Cd34
Eosinophil-Basophil-Mast cells:
Cd200r3, Fcer1a, Mcpt8, Prss34

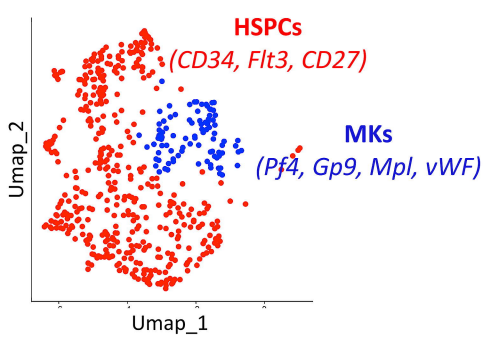

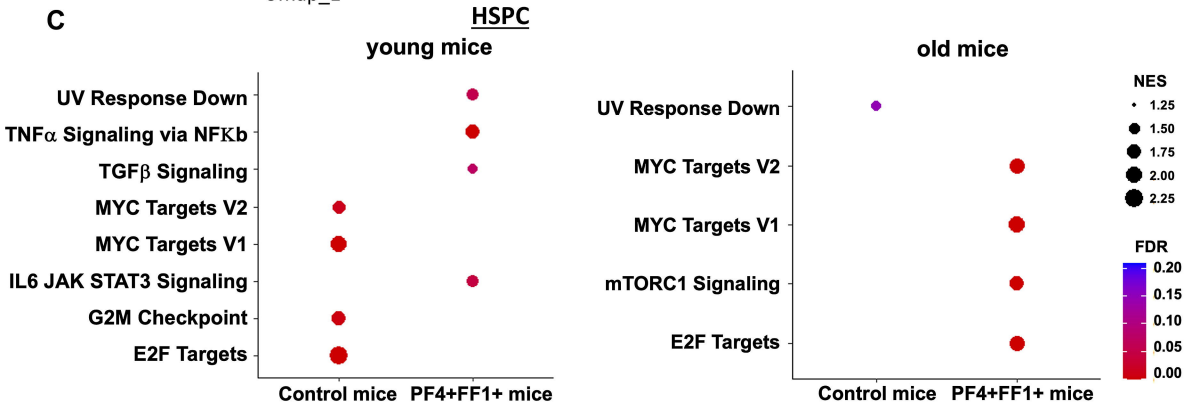

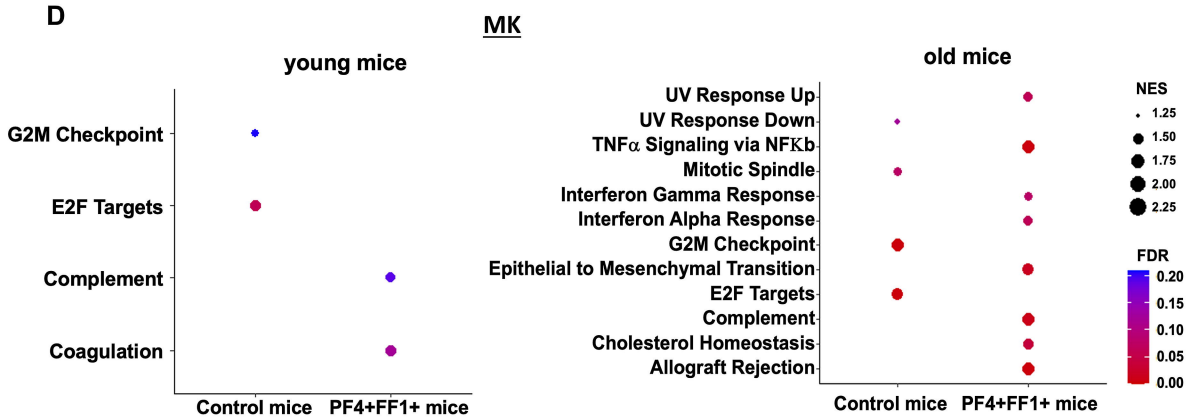

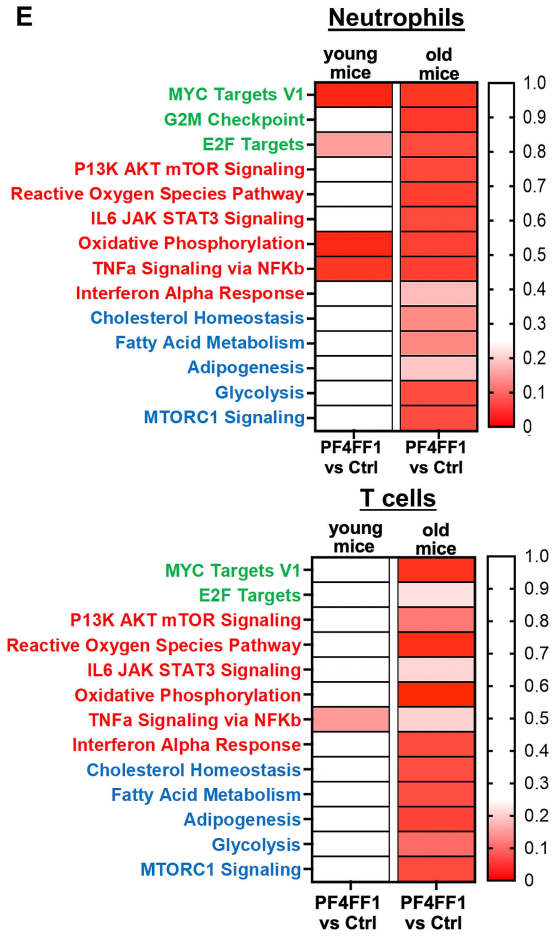

Figure 3

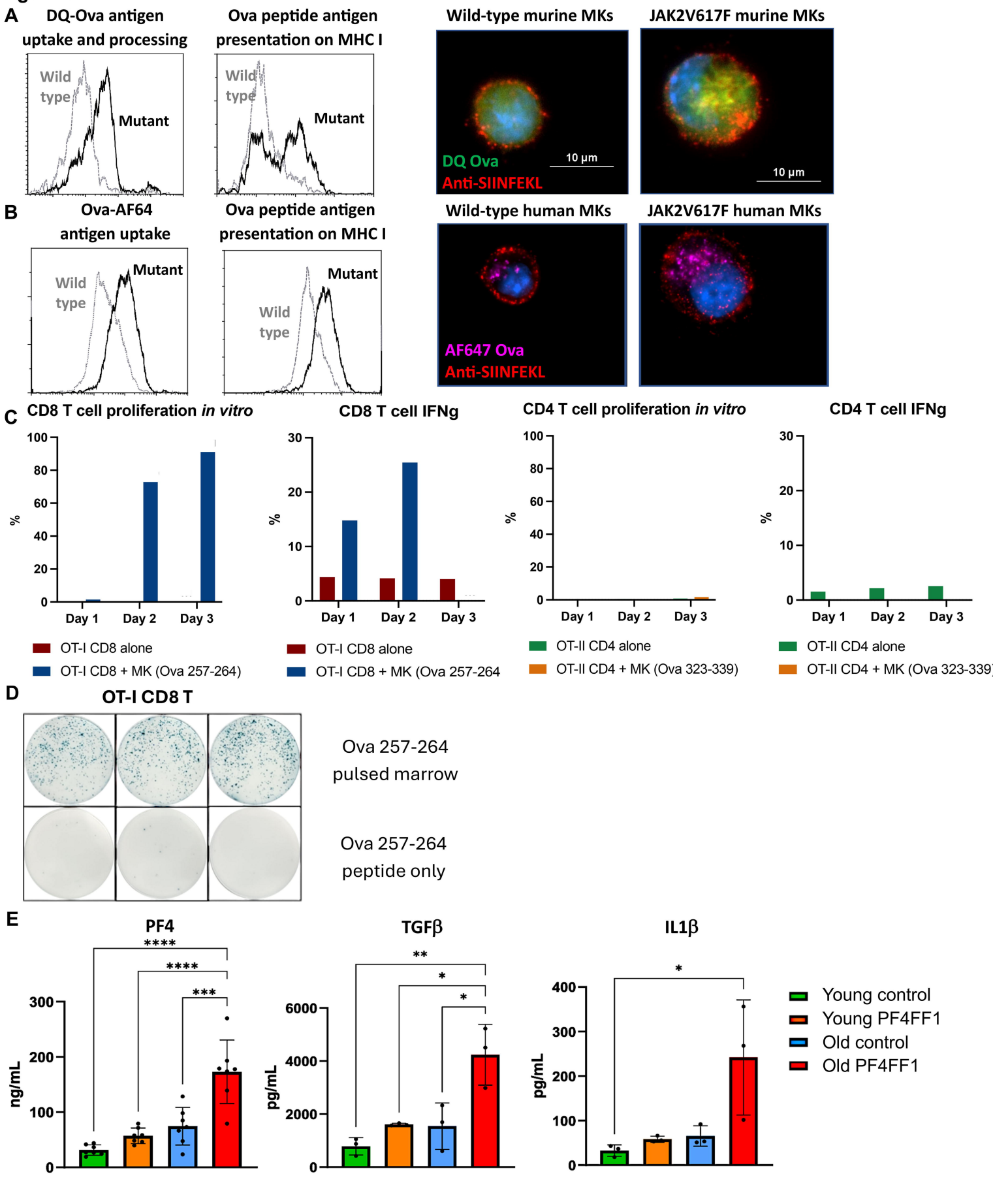
A
DQ-Ova antigen uptake and processing
Wild type
Mutant
Ova peptide antigen presentation on MHC I
Wild type
Mutant
Wild-type murine MKs
JAK2V617F murine MKs
DQ Ova
Anti-SIINFEKL
10 µm
10 µm
B
Ova-AF64 antigen uptake
Mutant
Wild type
Ova peptide antigen presentation on MHC I
Mutant
Wild type
Wild-type human MKs
JAK2V617F human MKs
AF647 Ova
Anti-SIINFEKL
C
CD8 T cell proliferation in vitro
%
Day 1
Day 2
Day 3
OT-I CD8 alone
OT-I CD8 + MK (Ova 257-264)
CD8 T cell IFNg
%
Day 1
Day 2
Day 3
OT-I CD8 alone
OT-I CD8 + MK (Ova 257-264
CD4 T cell proliferation in vitro
%
Day 1
Day 2
Day 3
OT-II CD4 alone
OT-II CD4 + MK (Ova 323-339)
CD4 T cell IFNg
%
Day 1
Day 2
Day 3
OT-II CD4 alone
OT-II CD4 + MK (Ova 323-339)
D
OT-I CD8 T
Ova 257-264 pulsed marrow
Ova 257-264 peptide only
E
PF4
ng/mL
TGFβ
pg/mL
IL1β
pg/mL
Young control
Young PF4FF1
Old control
Old PF4FF1

A

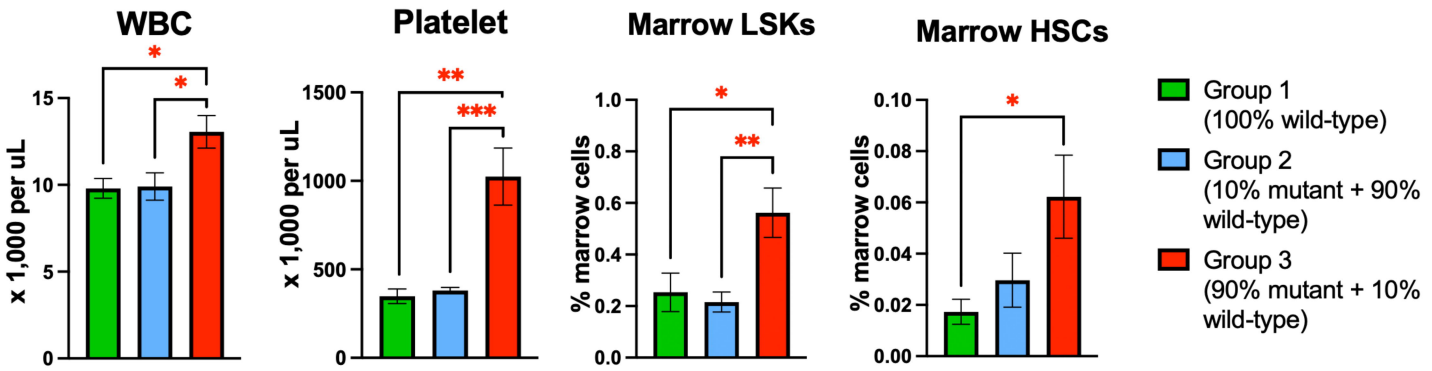

B

	Mutant: Wild-type donor ratio	Weeks after transplant	Blood count	Blood mutant donor chimerism	Marrow mutant donor chimerism	Marrow MKs	Marrow LSKs
Mouse A	10:90	16 wks	normal	2%	14%	0.78%	0.156%
Mouse B	90:10	12 wks	normal	63%	95%	0.56%	0.126%
Mouse C	90:10	16 wks	leukocytosis, thrombocytosis	95%	95%	3.73%	0.451%

C

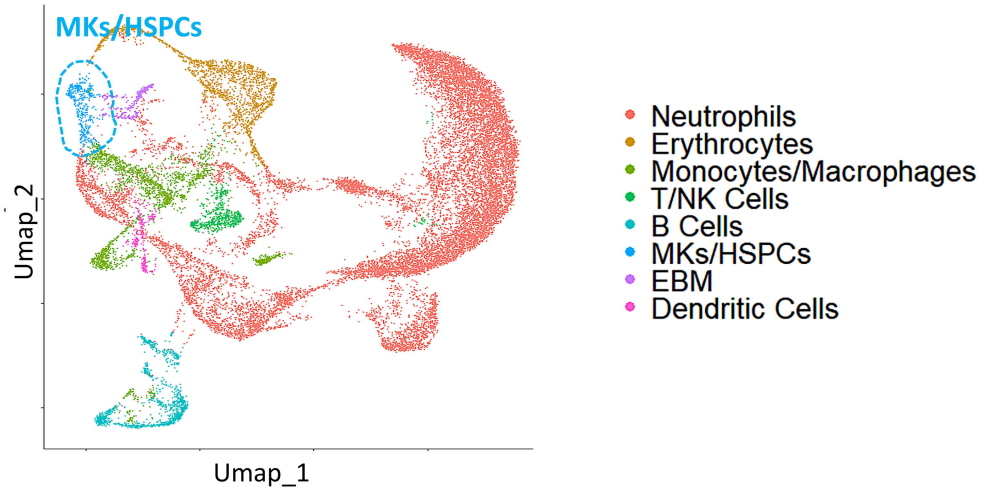

D

E

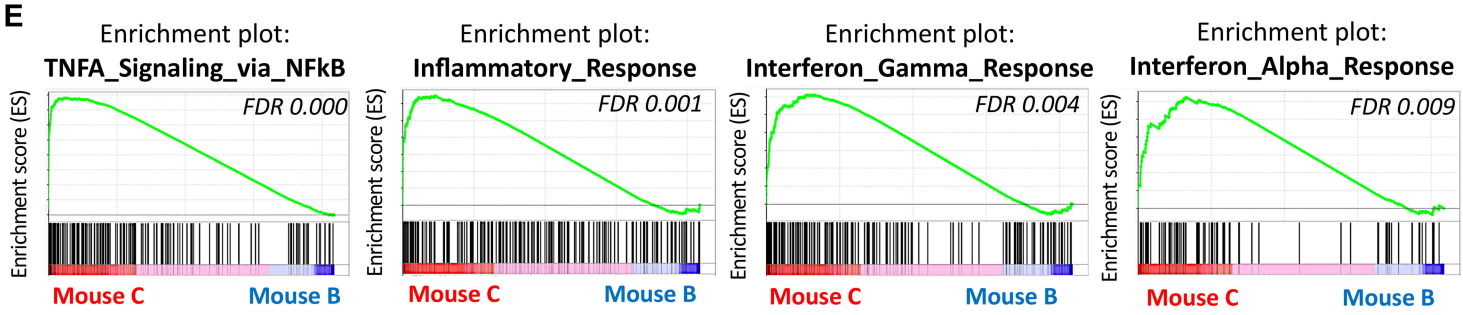

Figure 5.

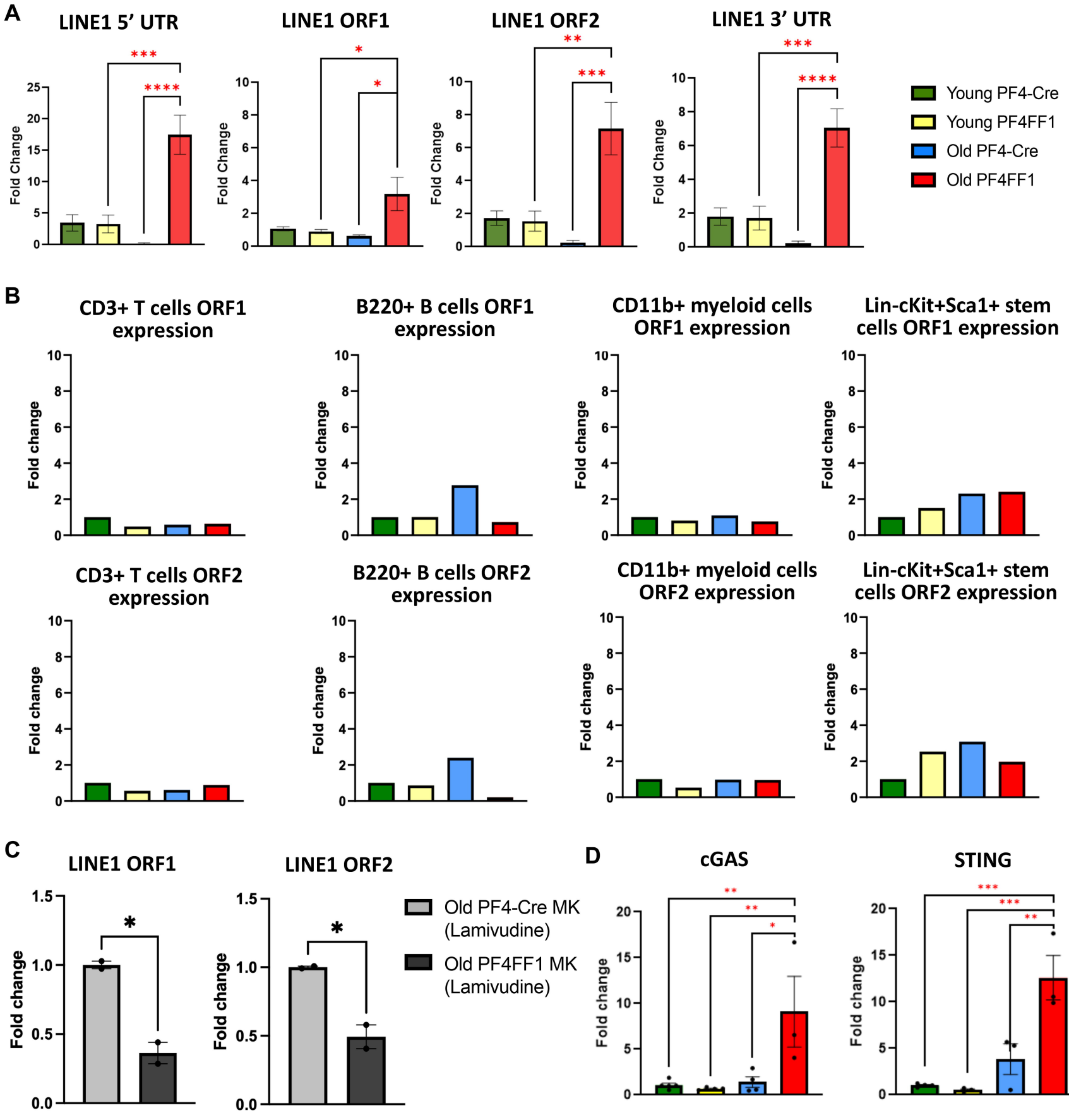
A
LINE1 5' UTR
LINE1 ORF1
LINE1 ORF2
LINE1 3' UTR
Fold Change
Young PF4-Cre
Young PF4FF1
Old PF4-Cre
Old PF4FF1
B
CD3+ T cells ORF1 expression
B220+ B cells ORF1 expression
CD11b+ myeloid cells ORF1 expression
Lin-cKit+Sca1+ stem cells ORF1 expression
CD3+ T cells ORF2 expression
B220+ B cells ORF2 expression
CD11b+ myeloid cells ORF2 expression
Lin-cKit+Sca1+ stem cells ORF2 expression
Fold change
C
LINE1 ORF1
LINE1 ORF2
Old PF4-Cre MK (Lamivudine)
Old PF4FF1 MK (Lamivudine)
D
cGAS
STING

Figure 6.

A

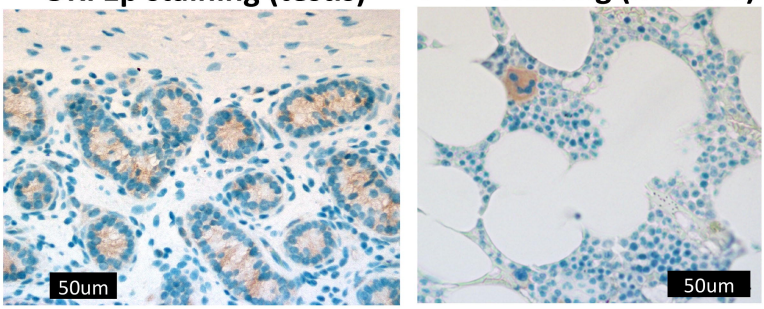

D

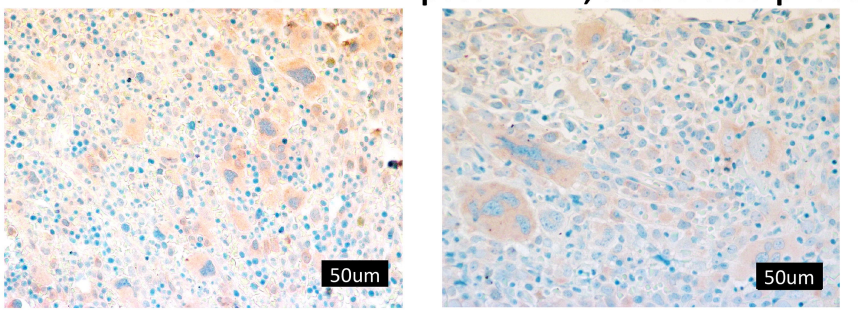

B

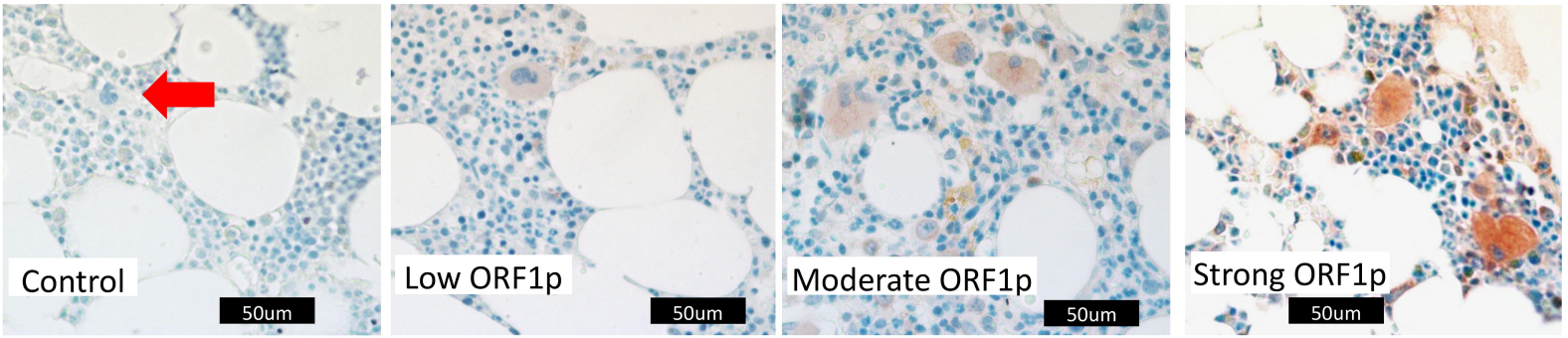

C

Patient no.	Gender	Age	MPN diagnosis	Mutation status	ORF1p-positive MK %
SL001	Female	78	MPN, nos	JAK2V617F	69%
SL002	Male	80	MPN, nos	ND	90%
SL003	Male	82	ET	ND	94%
SL004	Male	47	PMF	ND	95%
SL007	Female	78	PMF	JAK2V617F	69%
SL012	Female	80	ET	CALR	50%
SL016	Male	65	ET	CALR	41%
SL019	Male	58	ET	CALR	98%
SL025	Male	63	PV, evolving into MDS	JAK2V617F	100%
SL030	Male	72	PV	JAK2V617F	80%
SL035	Male	69	ET	JAK2V617F	73%
SL039	Female	76	PV	JAK2V617F	0%
SL046	Female	76	Post-PV MF (accelerated phase)	JAK2V617F	100%

ORF1p-positive MK% = number of ORF1p-positive MKs/total MKs [ORF1p-positive + ORF1p-negative] x 100%. An average of 70 MKs were evaluated per sample.

Supplementary materials and methods

Complete blood counts

Peripheral blood was obtained from the facial vein via submandibular bleeding and collected in EDTA tubes. The samples were then analyzed using a Vetscan Hm5 Hematology Analyzer (Abaxis) to determine the blood count.

Marrow cell isolation

Murine femurs and tibias were first harvested and cleaned thoroughly. Marrow cells were flushed into PBS with 2% fetal bovine serum using a 25G needle and syringe. Remaining bones were crushed with a mortar and pestle followed by enzymatic digestion with DNase I (25U/ml) and Collagenase D (1mg/ml) at 37 °C for 20 min under gentle rocking. Both flushed and digested marrow tissues were thoroughly dissociated by gentle and repeated mixing using a 10ml pipette to facilitate dissociation of cellular aggregates. Resulting cell suspensions were then filtered through a 70uM cell strainer.

Flow cytometry

Cells were counted and stained with antibodies by incubating cell suspensions at 4°C for 30 minutes in the dark. Samples were analyzed using a Cytoflex flow cytometer (Beckman Coulter, CA, USA) or sorted using a FACSAria III (BD biosciences, CA, USA). CD3 (clone 17A2, Biolegned), CD4 (clone GK1.5, Biolegend), CD8 (clone 53-6.7, Biolegend), CD25 (clone 3C7, Biolegend), FoxP3 (clone MF-14, Biolegend), CD45R/B220 (clone RA3-6B2, Biolegend), CD11b (clone M1/70, Biolegend), Ly6C (clone HK1.4, Biolegend), Ly6G (clone 1A8, Biolegend), CD41 (clone MWReg30, Biolegend), H-2D^{b} (clone KH95, Biolegned), IFNγ (clone XMG1.2, Biolegend), LINE1 ORF1p (clone ERP21844-108, Abcam), and Alexa Fluor 488 goat anti-rabbit IgG (A11008, Thermo Fisher, Waltham, MA) antibodies were used. Flow cytometry data were analyzed using Kaluza (Beckman Coulter).

Single cell RNA sequencing

Murine femurs and tibias were harvested and cleaned thoroughly. The bones were finely cut in PBS with 0.04% BSA. Cell suspensions were thoroughly homogenized by gentle and repeated mixing using a P1000 micropipette to facilitate dissociation of cellular aggregates. Resulting cell suspensions were then filtered through a 70uM cell strainer. Red blood cells were lysed twice using Red Blood Cell Lysing Buffer Hybri-Max (Sigma R7757). Final single bone marrow cells were washed and prepared in PBS with 0.04% BSA at a cell density of approximately 10^6 cells per 1 mL. Freshly isolated cell suspensions were immediately processed at the Single Cell Core Facility (Stony Brook University and Northport VA Medical Center) to generate single cell RNA sequencing libraries using Chromium Next GEM Single Cell 5′ Reagent Kit v2 (10x Genomics, Pleasanton, CA) according to the manufacturer's instructions. Briefly, cells, gel beads, and partitioning oil were loaded into a Chromium Next GEM Chip G, for a target recovery of 10,000 cells per sample. The chip was loaded into a Chromium Controller (10x Genomics) to generate Gel Bead-in-Emulsions (GEMs). After reverse transcription using a GEM–RT incubation protocol on a PCR cycler, the GEMs were broken using Recovery Agent (10x Genomics), and the cDNA was purified with DynaBeads MyOne Silane beads (10x Genomics), amplified by PCR for 13 cycles, and further purified with SPRIselect reagent (Beckman Coulter, Brea, CA, USA). The DNA concentration and amplicon size were measured using a TapeStation 4200 with the D5000 high sensitivity ScreenTape system (Agilent, Santa Clara, CA, USA). After fragmentation, end-repair, A-tailing, and size selection, the cDNA was ligated with adaptors and purified again with SPRISselect reagents, according to 10x Genomics instructions. Libraries were amplified by PCR with sample index oligonucleotide primers from the Chromium i7 Multiplex Kit (10x Genomics), for a total of 10 or 11 cycles, depending on the initial cDNA yield. The final PCR products were subjected to double-sided size selection with SPRISselect reagents. Library cDNA concentration and size was determined on the Agilent TapeStation 4200. cDNA libraries were sequenced using an NovaSeq XPlus, PE150 with the following sequencing settings: Read 1 – 151bp; i7 index – 10bp; Read 2 – 151bp (Novogene, Durham, NC, USA).

Single cell RNA sequencing data analysis

Raw sequencing data FASTQ files were aligned to the transcriptome assembly mm10-2020-A. Counts were obtained using the CellRanger count function, then analyzed using the Seurat 4.3.0 (R Foundation for Statistical Computing, Vienna, Austria). Correction of the gene expression matrix for ambient RNA contamination was done using the SoupX R package. Determination of doublets for exclusion was done using the DoubletFinder R

package. Cells were filtered to have at least 200 unique genes and less than 10% mitochondrial genes, as well as a log-normalized genes per UMI ratio of > 0.8. Data were normalized using the NormalizeData function using default parameters, and the top variable genes were identified using the FindVariableFeatures function with parameters of selection.method = "vst" and features = 3,000. After scaling the data using the ScaleData function, the most variable genes were used for principal component analysis (PCA) dimensionality reduction, using PCs 1:20 as determined by an Elbow Plot. Data were then integrated and the resulting clusters were visualized in a 2D Uniform Manifold and Approximation Projection (UMAP). Markers for identification were determined with a combination of literature review for markers, the use of marker resources such as CellMarker2.0 and Cell Taxonomy, information from companies such as Biolegend and R&D, and visualization of these markers in UMAP and violin plots. Differential expression data between clusters was retrieved using the FindMarkers function. The FindMarkers function was also used to retrieve differential expression data for between samples, ranked by p adjusted value.

In vitro murine MK antigen uptake, processing, and presentation

$CD41^+$ murine MKs were isolated from bone marrow using the EasySep Positive Selection Kit (StemCell Technologies, Cat. 17668) following the manufacturer's protocol. Isolated MKs were cultured overnight (~16 hours) in Serum-Free Expansion Media (SFEM, StemCell Technologies) supplemented with 25ng/mL recombinant mouse SCF and 25ng/mL recombinant mouse TPO at a density of $2x10^5$ MKs/ml in untreated round-bottom 96-well plates. Cells were then incubated with DQ-Ovalbumin (DQ-Ova, Thermo Fisher, Cat. D12053) at 200 ug/mL for 1 hour at 37°C. After incubation, cells were washed three times using cold PBS with 2% FBS. Cells were then stained with a monoclonal antibody targeting the OVA257-264 (SIINFEKL) peptide bound to H2-Kb of MHC class I (Invitrogen, Cat. 14574381) at 0.125 µg/test for 30 minutes at 4°C, followed by washing and staining with an Alexa Fluor 555-conjugated goat anti-mouse secondary antibody (Invitrogen, A-21422, 1:1000 dilution) for 30 minutes at 4°C. Cells were then washed, and fluorescence was analyzed by flow cytometry to assess antigen processing (DQ-Ova fluorescence is activated upon proteolytic cleavage) and antigen presentation (detected by binding of the anti-SIINFEKLE antibody to MHC I). For immunofluorescence imaging, cells were fixed with 4% PFA for 10 minutes at room temperature, washed, and stained with DAPI (2ug/mL) for 10 minutes at room temperature. Cells were then washed, cytospun onto a glass slide, and imaged using a Nikon Ts2R-FL microscope.

A similar protocol was applied to human $CD41^+$ MKs differentiated from iPS cell lines. In brief, iPS-differentiated MKs were cultured in SFEM containing 50ng/mL recombinant human SCF and 50ng/mL recombinant human TPO. Cells were incubated with Ovalbumin conjugated with an AF647 for 2 hours at 37ºC to assess antigen uptake. Antigen processing and presentation were evaluated by staining with the OVA257-264 (SIINFEKL)-H2-Kb MHC class I antibody, followed by flow cytometry analysis.

Cytokine Antibody Array

A membrane array was used for simultaneous detection of 62 different mouse cytokines according to the manufacturer's protocol (ab133995, Abcam, Cambridge, MA). Briefly, murine $CD41^+$ MKs were isolated using the column-free magnetic EasySep™ system (StemCell Technologies) and lysed in cell lysis buffer. Pooled MK cell lysate from young PF4-cre control mice (n=2), young PF4FF1 mice (n=2), old PF4-cre control mice (n=4), and old PF4FF1 mice (n=4) containing 250ng protein was incubated with the membrane overnight after appropriate blocking of the membrane. After washing, the detection antibody was applied to the membrane and immunoblot images were captured using a Bio-Rad ChemiDoc™ imaging system (Hercules, CA). The intensity of each spot was quantified using the ImageJ® software (National Institute of Health, Bethesda, MD).

Measurement of marrow plasma cytokines

Bone marrow plasma was collected by flushing 0.5mL of PBS into the marrow cavity of a single femur. The fluid was collected and centrifuged at 2,000 g for 15min to remove cell debris. For measurement of Platelet factor 4 (PF4) and Transforming growth factor beta **(**TGFβ) levels, samples underwent an additional centrifugation step to ensure complete platelet removal. The resulting marrow plasma was aliquoted and stored at -80℃ until further analysis. Cytokines levels were measured using ELISA kits following the manufacturer's instructions: PF4 (R&D Systems, Cat. MCX400), TGFβ (R&D Systems, Cat. DB100C), IL1β (R&D Systems, Cat. MLB00C), TNFα (R&D Systems, Cat. MTA00B-1), IL6 (R&D Systems, Cat. M6000B-1) ELISA kit according. All samples were analyzed in duplicate.

Real-time quantitative polymerase chain reaction

The Azure Cielo 6 Real-time PCR system (Azure Biosystems) was used for all experiments. Total RNA was isolated using the RNeasy mini kit (Qiagen) and was digested with RNase-free DNase (Qiagen). The RNA was then reverse transcribed to cDNA using the high-capacity cDNA reverse transcription kit (Thermo Fisher) following the manufacturer's protocol.

The Power SYBR Green PCR Master Mix (Thermo Fisher) was used for real-time quantitative polymerase chain reaction (qPCR) to verify differential expression of LINE1 using primers designed on the consensus sequence of the L1MdA and L1Tf families: 5'UTR (forward: CTGCCTTGCAAGAAGAGAGC; reverse: AGTGCTGCGTTCTGATGATG), ORF1 (forward: ATCTGTCTCCCAGGTCTGCT; reverse: TCCTCCGTTTACCTTTCGCC), ORF2 (forward: GCTTCGGTGAAGTAGCTGGA; reverse: TTCGTTAGAGTCACGCCGAG), and 3'UTR (forward: AGCCAAATGGATGGACCTGG; reverse: AAGGAGGGGCATAGTGTCCA) elements[1]. GAPDH (forward: CGGCCGCATCTTCTTGTG, reverse: GTGACCAGGCGCCCAATA) was used as the normalization controls. The TaqMan® Gene Expression Assays (ThermoFisher) were used for real-time qPCR to verify differential expression of cGAS (Mm01147496_m1), STING (Mm01158117_m1), and JAK2 (Hs01078117_m1). Relative fold changes compared to control samples was calculated by the $2^{\Delta\Delta CT}$ method. All assays were performed in triplicate.

Human iPS cell culture and differentiation into megakaryocytes

The BC1 iPS cell line (JAK2 wild-type, healthy donor-derived) and PVB1.4 iPS cell line (JAK2V617F homozygous, PV patient-derived) were maintained under feeder-free conditions on vitronectin-coated plates (0.5 µg/cm², Gibco, Cat. A14700) using Essential 8™ Medium (Gibco, Cat. A1517001). Cells were passaged as small clumps using 0.5 mM EDTA and maintained in an undifferentiated state. To enhance post-thaw viability, RevitaCell™ Supplement (Gibco, Cat. A2644501) was added for the first 24 hours, after which the medium was changed every 1–2 days without RevitaCell.

Hematopoietic differentiation: iPS cells were differentiated into hematopoietic cells using a modified spin-embryoid body (EB) method under feeder- and serum-free conditions[2-4]. On **Day 0**: iPS cells were dissociated into single cells using Accutase (Sigma, Cat. A6964) and seeded into 96-well untreated round-bottom plates at 3000 cells/50uL per well in StemSpan™ SFEM medium (StemCell Technologies, Cat. 09650) supplemented with RevitaCell™ (1x), 10ng/mL recombinant human FGF-2 (Peprotech, Cat. 100-18B), and 10ng/mL recombinant human BMP4 (R&D Systems, Cat. 314-BP). Plates were centrifuged at 400g for 5 minutes (no break) at room temperature to form EBs. On **Days 2, 5, 8, and 11**: 50uL of fresh StemSpan™ SFEM medium was added to each well, containing the final concentrations of 10ng/mL rhFGF-2, 10ng/mL rhBMP4, 50ng/mL recombinant human SCF (R&D Systems, Cat. 255-SC), and 10ng/mL recombinant human VEGF-A (Peprotech, Cat. 100-20) (Note: on Day 8, 100uL of media was removed from each well before adding fresh medium). On **Day 11**, 50uL of fresh StemSpan™ SFEM medium containing the final concentrations of 10ng/mL rhFGF-2, 10ng/mL rhBMP4, 50ng/mL rhSCF, 10ng/mL rhVEGF-A, and 20ng/mL recombinant human TPO (StemCell Technologies, Cat. 78210). **Day 14-18**: suspended hematopoietic cells were harvested and filtered through a 100um cell strainer (Miltenyi Biotec, Cat. 130-110-917) to remove remaining EBs.

Megakaryocytic differentiation: The harvested hematopoietic cells were cultured in StemSpan™ SFEM medium supplemented with 50ng/mL rhTPO, 10 ng/mL recombinant human IL-11 (Peprotech. Cat. 200-11), and 20 ng/mL rhSCF. Cells were seeded at 5 x 10^5/mL in flat-bottom, non-treated plates for 5 days, with medium replenishment on Day 3. MKs were enriched by $CD41^+$ positive selection using the EasySep Positive Selection Kit (StemCell Technologies, Cat. 17662), following the manufacturer's protocol.

Nested allele-specific PCR for JAK2V617F-positive iPS cells

Genomic DNA was isolated using the DNeasy Blood and Tissue Kits (Qiagen, Cat. 69504). For amplification of the *JAK2* gDNA, the PCR primers 5′-GATCTCCATATTCCAGGCTTACACA-3′ and 5′-TATTGTTTGGGCATTGTAACCTTCT-3′, which cover exon 14 of the human *JAK2* gene. The PCR product is further amplified using nested and allele-specific primers: 5'-CCTCAGAACGTTGATGGCA-3', 5'-ATTGCTTTCCTTTTTCACAAGA-3', 5'-GTTTTACTTACTCTCGTCTCCACAAAA-3' (JAK2V617F mutation-specific), and 5'-AGCATTTGGTTTTAAATTATGGAGTATATG-3' (JAK2 wild type-specific). The final PCR products were analyzed on 2.0% agarose gels. A 279-bp product indicated allele-specific JAK2V617F-positive, whereas a 229-bp product denoted allele-specific wild-type product.

Immunohistochemistry

Formalin-fixed, paraffin-embedded (FFPE) bone marrow sections were stained for LINE-1 ORF1p and CD41 using an adapted immunohistochemistry (IHC) protocol[5]. Slides were baked at 60℃ for 20-30min to melt paraffin, followed by sequential wash with xylene, 100%, 95%, 70%, and 50% ethanol, and running tap water for rehydration. Heat-induced antigen retrieval was performed by immersing slides in Reveal Decloaker (Biocare Medical, RV1000M, pH 6) and heating in a steamer at 98°C for 25 minutes. After cooling to room temperature, slides were washed in TBST for 5 minutes and blocked with 1% bovine serum albumin (BSA) in TBST for 30 minutes. Primary antibodies were incubated overnight at 4°C in a humidity chamber: mouse anti-human LINE-1 ORF1p (clone 4H1, Millipore Sigma, MABC1152) at 1:800 dilution (0.625 µg/mL), or rabbit anti-human CD41 (clone EPR4330, Abcam, ab134131) at 1:2000 dilution (0.325 µg/mL). After three TBST washes, endogenous peroxidase activity was quenched with 3% hydrogen peroxide for 5 minutes, followed by additional TBST washes. Secondary antibody incubation was performed for 1 hour at room temperature in a humidity chamber using IgG HRP-linked anti-mouse (Cell Signaling Technology, Cat. 7076) or anti-rabbit (Cell Signaling Technology, Cat. 7074) at 1:100 dilution. Following three TBST washes, detection was performed using the DAB substrate kit (Abcam, ab64238) with DAB enhancer (Abcam, ab675), incubating for 1 minute for both LINE-1 ORF1p and CD41. Slides were washed in water to stop the reaction, counterstained with Mayer's hematoxylin (G-Biosciences, Cat. 786-1264), and treated with a bluing solution (10g magnesium sulfate ($MgSO_4$) and 0.67g sodium bicarbonate ($NaHCO_3$) in 1 L of deionized water). Dehydration was performed through increasing ethanol concentrations, followed by xylene. Slides were coverslipped using Limonene mounting medium (Abcam, AB104141). LINE-1 ORF1p intensity was evaluated using a four-level semiquantitative scale: 0 = negative; 1 = low; 2 = intermediate; and 3 = high.

Quantification and statistical analysis

Statistical analyses were performed using GraphPad Prism 9 (San Diego, CA) and *R* software. All measurements were taken from distinct samples. Except for the scRNAseq experiments, all assays were performed independently at least twice. Two-way ANOVA was used to compare blood cell counts between wild-type control and $Pf4^{+}FF1^{+}$ mice, while the two-tailed Student's *t*-test was applied to determine statistical significance between groups. For *in vivo* experiments, randomization and blinding were not used. Sample size for animal studies were chosen to ensure a balance between the minimum numbers necessary for efficient analysis while accounting for biological variability. Figures were generated using GraphPad Prism 9, R software, and BioRender.com.

1. De Cecco M, Ito T, Petrashen AP, et al. L1 drives IFN in senescent cells and promotes age-associated inflammation. Nature 2019;566(7742):73-78. DOI: 10.1038/s41586-018-0784-9.
2. Ye Z, Zhan H, Mali P, et al. Human-induced pluripotent stem cells from blood cells of healthy donors and patients with acquired blood disorders. Blood 2009;114(27):5473-80. DOI: 10.1182/blood-2009-04-217406.
3. Liu Y, Wang Y, Gao Y, et al. Efficient generation of megakaryocytes from human induced pluripotent stem cells using food and drug administration-approved pharmacological reagents. Stem Cells Transl Med 2015;4(4):309-19. DOI: 10.5966/sctm.2014-0183.
4. Li Y, Jin C, Bai H, et al. Human NOTCH4 is a key target of RUNX1 in megakaryocytic differentiation. Blood 2018;131(2):191-201. DOI: 10.1182/blood-2017-04-780379.
5. Sharma R, Rodic N, Burns KH, Taylor MS. Immunodetection of Human LINE-1 Expression in Cultured Cells and Human Tissues. Methods Mol Biol 2016;1400:261-80. DOI: 10.1007/978-1-4939-3372-3_17.

Supplementary figures

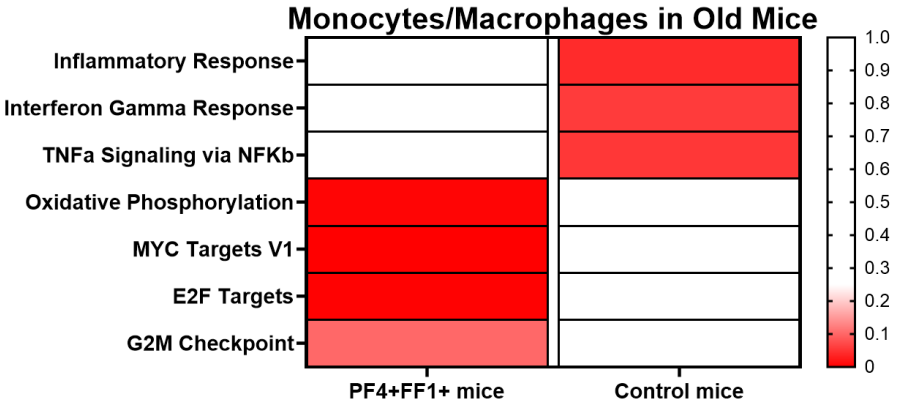

Supplementary Figure 1. GSEA analysis of monocytes/macrophages in old $Pf4^{+}FF1^{+}$ (left) and control (right) mice.

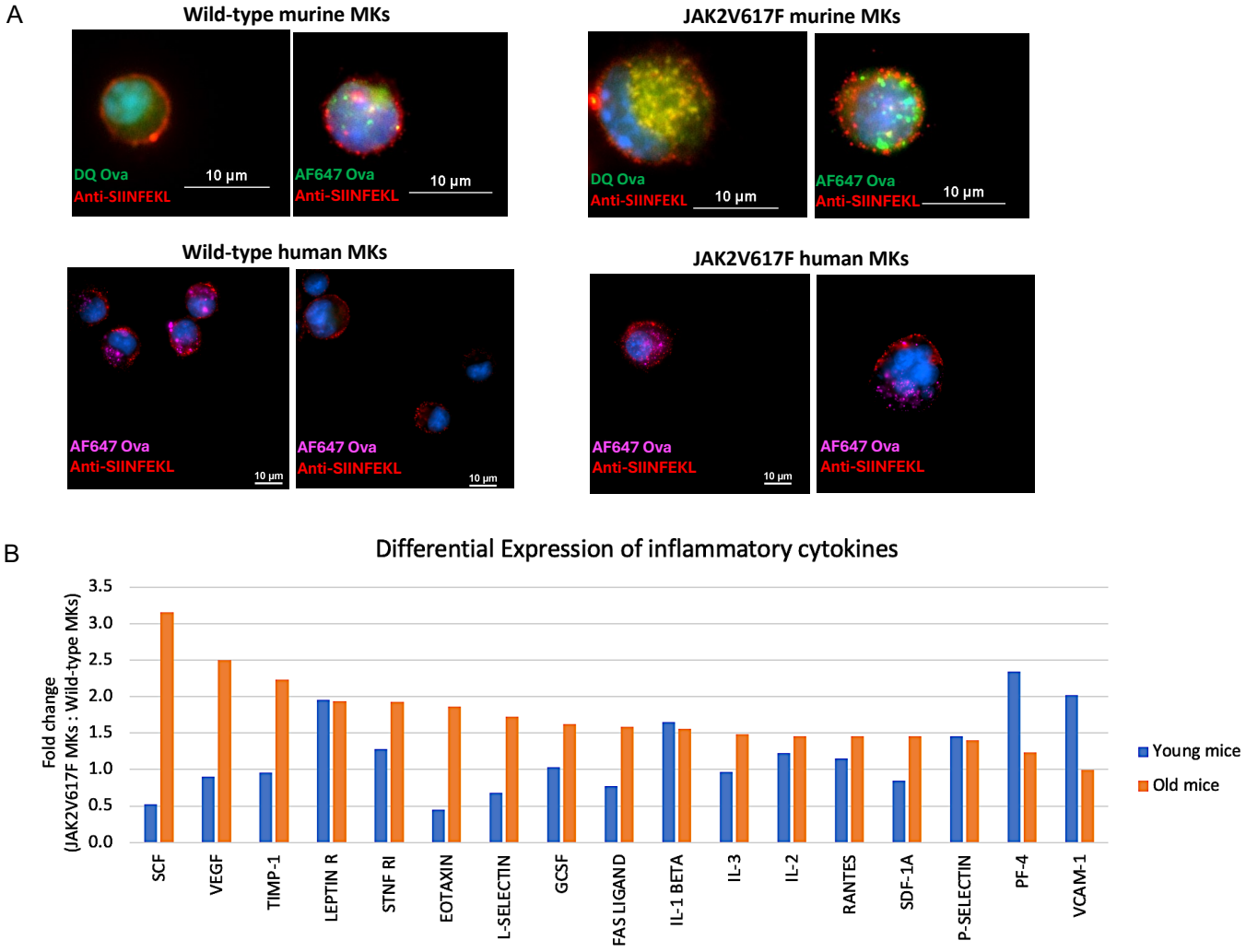

Supplementary Figure 2. (**A**) Additional fluorescence images showing wild-type and JAK2V617F mutant murine (top) and human (bottom) MKs internalizing Ovalbumin and presenting OVA peptide antigens on MHC I molecules. (**B**) Selected cytokine array data illustrating increased expression of many inflammatory cytokines in JAK2V617F MKs from aged $Pf4^{+}FF1^{+}$ mice compared to wild-type MKs from aged-matched control mice (pooled MK cell lysate from 2-4 mice per group).

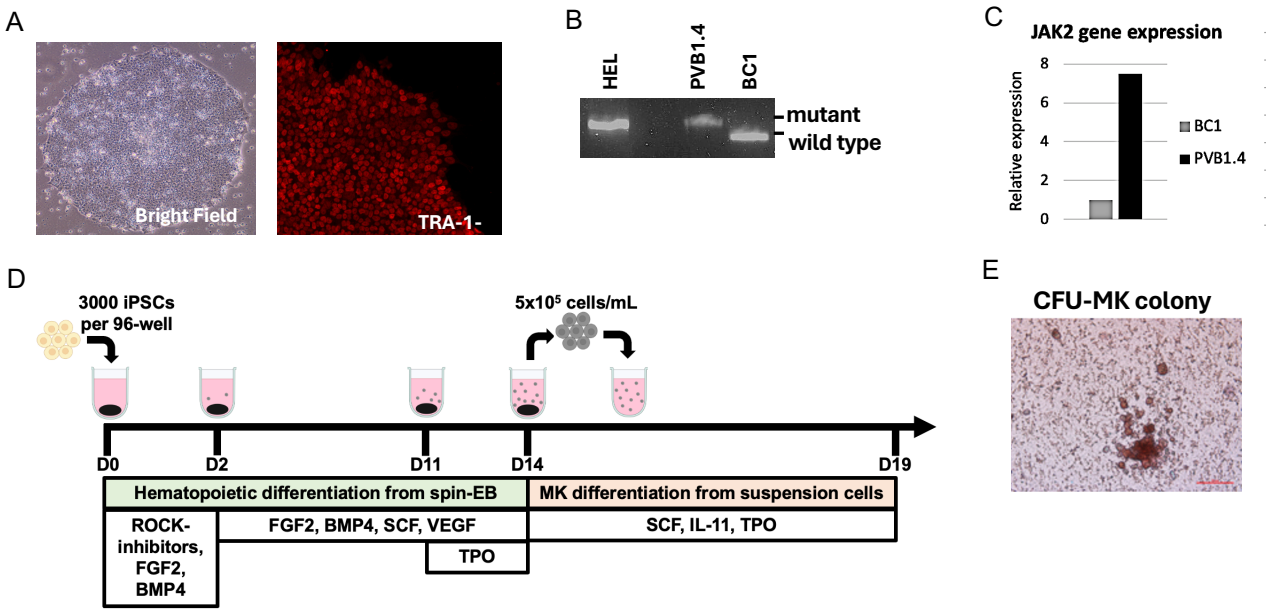

Supplementary Figure 3. iPS cell line model for studying human MK functions. (**A**) Immunofluorescence staining of iPS colonies showing expression of the undifferentiated cell markers TRA1-60. (**B**) Detection of wild-type JAK2 allele (229bp) and JAK2V617F mutant allele (279bp) by nested allele-specific PCR. HEL: human erythroleukemia cell line (JAK2V617F mutant, positive control). (**C**) JAK2 gene expression in BC1 and PVB1.4 iPS cells measured by real-time qPCR. Gene expression is shown as fold-change relative to BC1, which was set as 1. (**D**) Schematic presentation of the hematopoietic and megakaryocytic differentiation strategy for human iPS cells. (**E**) Representative CFU-MK colony formation assay of iPS-derived $CD41^{+}$ MKs.

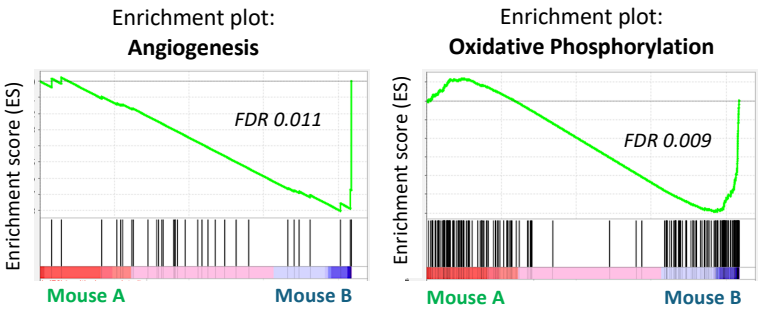

Supplementary Figure 4. Top gene sets significantly enriched in Mouse B (90% mutant, normal blood counts) MKs compared to Mouse A (10% mutant, normal blood counts) MKs.